2017

Mathematical Modeling and Capacity Fading Study in Porous Current Collector Based Lithium Ion Battery

Surendra Bajagain
South Dakota State University

MATHEMATICAL MODELING AND CAPACITY FADING STUDY IN POROUS CURRENT COLLECTOR BASED LITHIUM ION BATTERY

BY

SURENDRA BAJAGAIN

A thesis submitted in partial fulfillment of the requirements for the

Master of Science

Major in Electrical Engineering

South Dakota State University

2017

MATHEMATICAL MODELING AND CAPACITY FADING STUDY IN POROUS CURRENT COLLECTOR BASED LITHIUM ION BATTERY

This thesis is approved as a creditable and independent investigation by a candidate for the Master of Science in Electrical Engineering degree and is acceptable for meeting the thesis requirements for this degree. Acceptance of this thesis does not imply that the conclusions reached by the candidates are necessarily the conclusions of the major department.

Qiquan Qiao, Ph.D.
Thesis Advisor Date

Steven Hietpas, Ph.D.
Head, Electrical Engineering and Computer Science Date

Dean, Graduate School Date

I dedicate my thesis to my late grandfather Rishi Ram Bajagain for teaching me “Life is full of ups and downs, but we need to stay calm during both ups and downs of life.”

ACKNOWLEDGEMENTS

I would first like to express my gratitude to my thesis advisor and graduate coordinator, Dr. Qiquan Qiao for providing me the opportunity to work in his research group as a research assistant and his enormous help throughout this project. Without his continuous support and feedback, I would not have been able to stand in this position in a short span of time.

I am thankful to Electrical Engineering and Computer Science department for providing me the opportunity to be part of this esteemed department and financial support for my graduate education.

I would like to thank committee members Dr. Zhen Ni, Dr. Parashu Kharel and graduate faculty representative Dr. Christopher Chase for valuable suggestions and encouragement. Also, I would like to thank Raju Prased Ghimire for performing the experimental part of this work.

Equally, I can't stay without thanking Ashim Gurung, Ke Chen, and Rajesh Pathak, the seniors Ph.D. students for their continuous guidance towards mentoring the battery researches.

I am very thankful to my father, Khem Raj Bajagain and mother, Krishna Kumari Bajagain for their everlasting love and encouragement to achieve what I dreamt of.

Last but not the least I would like to thank all the members of Dr. Qiao research group.

CONTENTS

ABBREVIATIONS

Acronyms

$DAEs$	Differential algebraic equations
DOD	Depth of Discharge
EAM	Electrode Averaged Model
$ECMs$	Equivalent Circuit Models
EMF	Electromotive force
EMs	Electrochemical Models
FDM	Finite difference method
$Li-ion$	Lithium ion
$LIBs$	Lithium- ion batteries
$P2D$	Pseudo two dimensional
$PDEs$	Partial differential equations
$RMSE$	Root mean square error
SEI	Solid electrolyte interface
SOC	State of Charge
SOH	State of health
SSE	Sum of square error
SVM	State Values Model

Greek letters

α_a	Anodic transfer coefficients of electrode reaction

α_c	Cathodic transfer coefficients of electrode reaction
δ_{film}	SEI layer thickness (m)
ε_k	Porosity of electrode k
ε_δ	Porosity of deposit
ε_{cc}	Porosity of current collector
$\varepsilon_{f,k}$	Volume fraction of fillers in region k
ε_{SEI}	Volume fraction of SEI layer
η	Overpotential (V)
η_{side}	Overpotential for side reaction
$\kappa_{eff,k}$	Effective ionic conductivity of the electrolyte in region k (Sm^{-1})
κ_{SEI}	Conductivity of SEI layer (Sm^{-1})
Ω_{SEI}	Initial resistance of SEI layer (Ωm^2)
ϕ_s	Solid-phase potential(V)
ρ_k	Density of region k (kgm^{-3})
$\sigma_{eff,k}$	Effective electronic conductivity of solid phase electrode k (Sm^{-1})
σ_k	Electronic conductivity of solid phase electrode k (Sm^{-1})
θ_k	Dimensionless concentration of Li^+ ions in the intercalation particle of electrode k
ζ_k	Morphology of the side reaction product formed

List of symbols

$brugg_k$	Bruggeman coefficient of region k
$c_{e,k}$	Electrolyte concentration in region k ($molm^{-3}$)

$c_{s,k}$	Concentration of Li^+ ions in the intercalation particle of electrode k ($molm^{-3}$)
$c^*_{s,k}$	Surface concentration of electrode k ($molm^{-3}$)
$c^{avg}_{s,k}$	Solid-phase average concentration of electrode k ($molm^{-3}$)
$D_{eff,k}$	Effective diffusion coefficient in region k
$D_{s,k}$	Li^+ diffusion coefficient in the intercalation particle electrode k (m^2s)
F	Faraday's constant ($Cmol^{-1}$)
G_{film}	Film resistance (Ωm^2)
I	Applied current density (Am^{-2})
i_{os}	Exchange current density for solvent reduction reaction (Am^{-2})
J_k	Wall-flux of Li^+ on the intercalation particle of electrode k ($molm^{-2}s$)
J_{lpl}	Reaction current for lithium plating (Am^{-3})
J_{side}	Reaction current for solvent reduction reaction (Am^{-3})
K_k	Reaction rate constant of electrode k ($molmol^{-1}m^3$)
L	Total thickness of battery
M_k	Mass of region k (kgm^{-2})
M_{SEI}	Molecular weight of SEI layer ($kgmol^{-1}$)
N	Cycle number
R	Universal gas constant
r	Radial coordinate (m)
R_P	Spherical particle radius
T	Absolute temperature (K)

t_+	Li^+ transference in electrolyte
U_k	Open-circuit potential of electrode k (V)
x	Spatial coordinate (m)

Subscripts

cc	Current collector
eff	Effective
max	Maximum
min	Minimum
n	Negative electrode
p	Positive electrode
s	Solid phase
sep	Separator
$side$	Side reaction

LIST OF FIGURES

LIST OF TABLES

ABSTRACT

MATHEMATICAL MODELING AND CAPACITY FADING STUDY IN POROUS CURRENT COLLECTOR BASED LITHIUM ION BATTERY

SURENDRA BAJAGAIN

2017

Lithium ion (Li-ion) batteries are primary energy storage devices especially in electronic gadgets, electric vehicles and for stationary storage of intermittent renewable energy. These applications demand durable Li-ion batteries with higher energy density. Energy density can be increased either by finding novel electrode materials or by modifying the existing design of the battery. The electrode materials or modified design should not only increase energy density, but also should control the capacity fading of the battery.

In this work, existing mathematical model of Li-ion battery was adjusted in the case of the porous current collector. The discharge performance and capacity fading of the porous current collector based Li-ion battery was compared with non-porous current collector Li-ion battery. The electrode averaged model (EAM) was used to simulate the discharge performance of the battery. The capacity fade was compared by comparing the film growth, change of initial electrode state of charge (SOC) and change in solid phase diffusion coefficient with cycling. Both simulation and experimental results have shown the porous current collector based Li-ion battery achieves greater than the theoretical specific capacity of electrode active materials for the first few cycles of operations. In this work, Lithium titanate was considered as an electrode active material which has a

theoretical specific capacity of 175 mAh/g. Simulation and experiment have predicted specific capacities of 238 mAh/g and 235 mAh/g respectively in the case of the porous current collector. Simulation result showed the porous current collector Li-ion batteries reaches the end of useful life after 100 more cycles than the non-porous current collector batteries under similar conditions of operation.

CHAPTER 1 INTRODUCTION

1.1 Background

Industrialization has improved the quality of life of world population. Improved life standards have increased the energy consumption. *International Energy Outlook 2016* (IEO2016) released by the U.S. Energy Information Administration states that world energy consumption will grow by 48% between 2012 and 2040 [1]. Population growth and per capita consumption growth are two major causes for the energy consumption growth. As of now, fossil fuels are the main sources of energy. Fossil fuels are non-renewable and burning of fossil fuels produces carbon dioxide (CO_2). About 21.3 billion tonnes of CO_2 are produced by burning fossil fuels per year [2]. Natural processes can absorb only about half of that amount and hence there is a net increase of 10.65 billion tonnes of CO_2 per year [3]. CO_2 is a greenhouse gas and contributes to global warming. Figure 1.1 shows the percentage of CO_2 emissions in different sectors, where 43.9% of total emission are from electricity generation and heating. To cope with energy growth and to control the emission of CO_2 researchers are focusing on the development of renewable energy sources and green energy technologies.

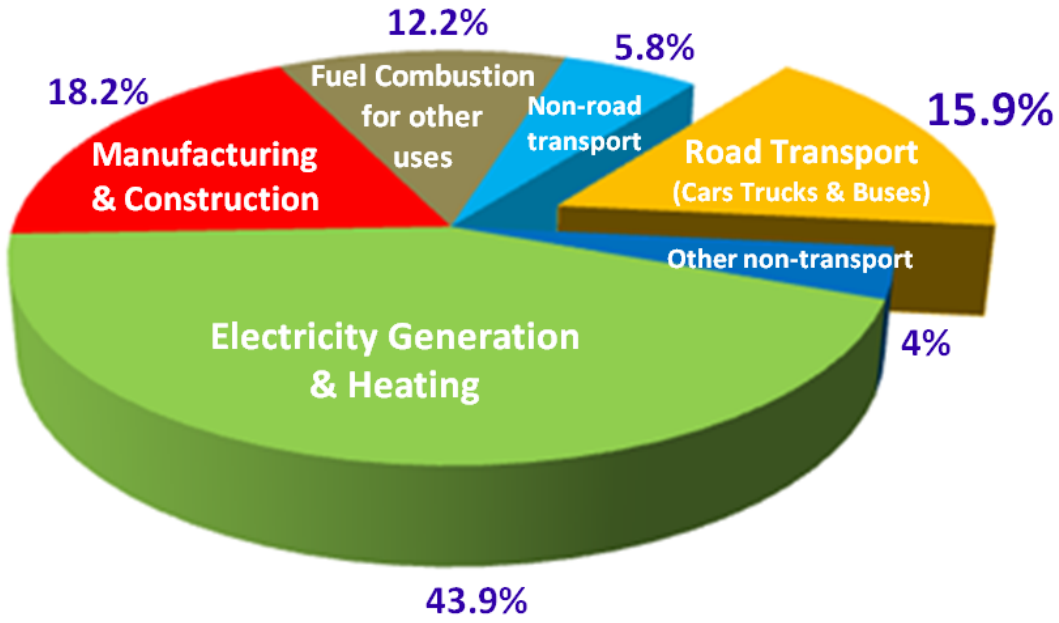

Figure 1.1. CO_2 emission in different sectors [4].

As the world focuses on the development of alternative energy sources and green technologies due to global warming and the prediction that the fossil fuels are running out soon, the development of energy storage technology is gaining popularity. Research is being conducted for the design of cheap, efficient, and self-charging energy storage devices through solar cells [5].

In electricity grid demand must be met by the power supply at any moment. Energy storage can act as a balancing agent when the supply needs to be adjusted due to predictable changes in the demand or unexpected changes from equipment overloads and storms. The balancing act of energy storage increases the grid flexibility and reliability. Further, energy storage can be used to smooth the electricity from intermittent renewable energy sources like solar and wind. The energy storage device has a fast response which is used to maintain the stability of the grid when unexpected load increase occurs on the grid.

Energy storage devices play a vital role to ensure the stability of power supply in off-grid applications such as camping, microgrids. Batteries, flywheels, fuel cells, supercapacitors etc. are some of the energy storage devices. Battery modeling is the focus of this thesis.

Volta in 1800 discovered certain fluids, when used as a conductor, would generate electricity, which paved a path to the invention of the first voltaic cell commonly known as a battery. Ever since the concept of storing energy electrochemically began. At the end of the nineteenth century, batteries were primary sources of electricity before electrical generators and electrical grids were developed.

Initial batteries were non-rechargeable, primary cell, meaning they were designed for one-time use. First rechargeable battery, secondary cell, based on lead-acid chemistry was invented in 1859 by the French physician Gaston Planté. Lead-acid chemistry is still widely in use. Lead-acid batteries are cheap, robust, can deliver very high currents and can be stored indefinitely without the electrolyte. However, they are heavy, bulky, unsuitable for fast charging, and are susceptible to sulphation under low electrolyte conditions.

As demand for smaller, lighter and deep cycle life rechargeable batteries have increased, different battery chemistries have been developed. Nickel-cadmium (NiCd), Nickel Metal Hydride (NiMH), Li-ion chemistries are commonly used [6]. NiCd batteries are capable of deep cycling. Also, they are smaller and lighter than lead-acid batteries, but they require periodic maintenance, shows memory effect that reduces usable capacity with time and they contain cadmium which is not environmentally friendly. NiMH batteries are replacing NiCd batteries. However, they have high self-discharge rate. Li-ion chemistries provide one of the best tradeoffs in terms of power density, low weight, cell voltage and low self-discharge [7]. As shown in figure 1.2, Li-ion is the best chemistry in terms of

volumetric energy density among the existing chemistries. Furthermore, they are the lightest and smallest among the existing batteries.

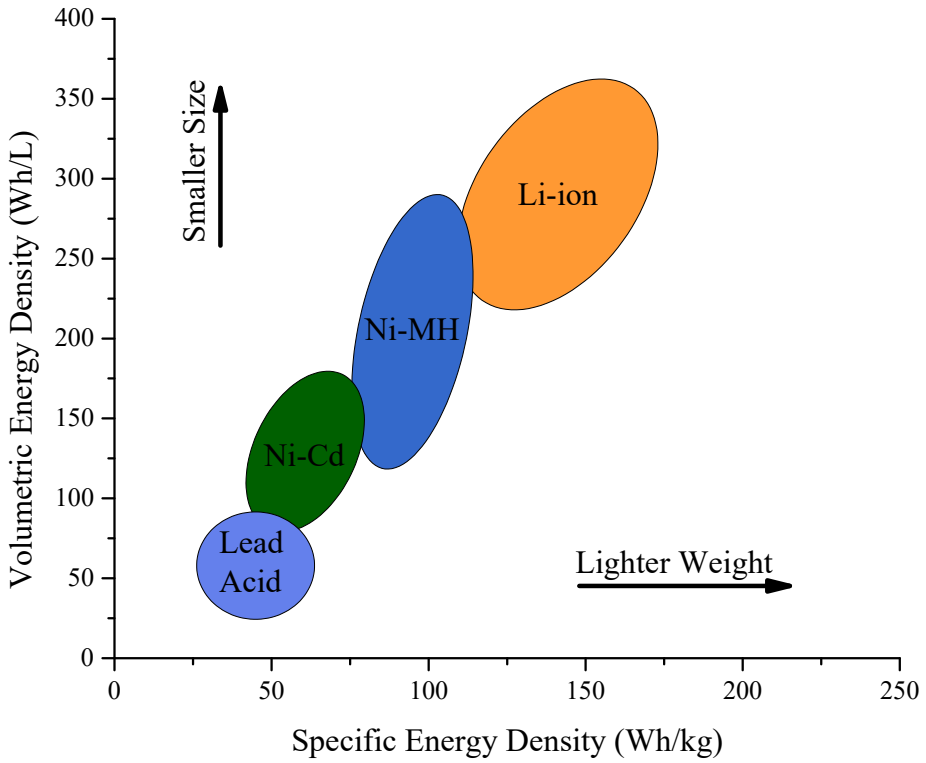

Figure 1.2. Diagram comparing the rechargeable battery technologies as a function of volumetric and specific energy densities [8].

Rechargeable Li-ion batteries (LIBs) were first commercialized by Sony in 1991 [9]. Since launch, LIBs have had an increasing market share due to increased usage of electronic devices and the progress of electric and hybrid vehicles. Figure 1.3 shows the demand for Li-ion batteries for two decades. It is expected that nearly 100 GW hours of Li-ion batteries are required to meet the needs from consumer use and electric-powered vehicles with the latter taking about 50% of Li-ion battery sale by 2018 [10].

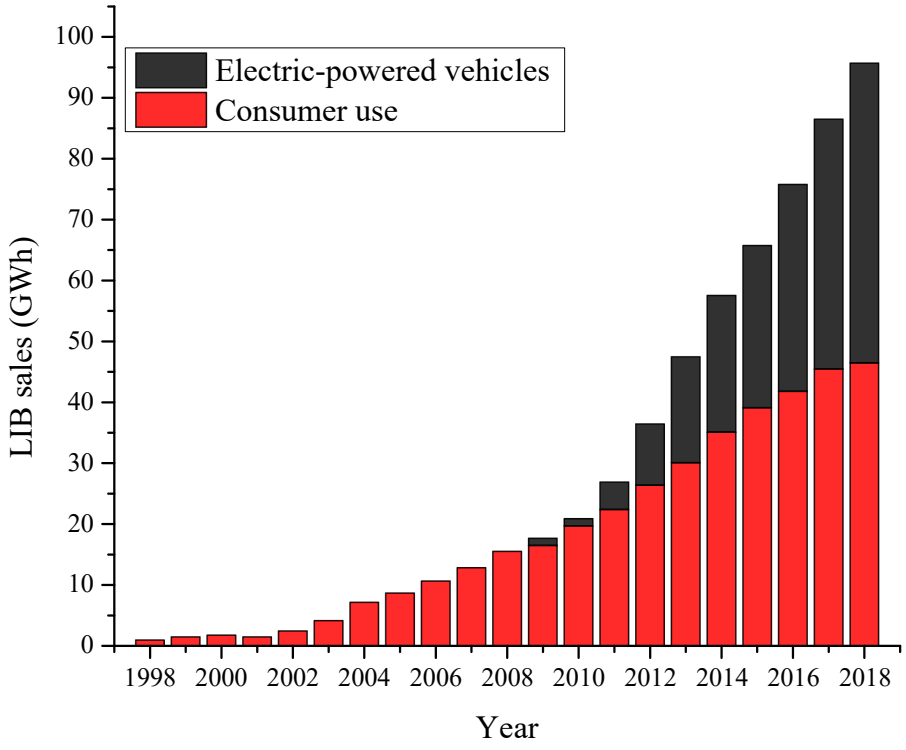

Figure 1.3. Demand for Li-ion batteries in two decades [11].

Li-ion batteries are dominant in portable electronic devices like cell phones, laptops, and are becoming suitable energy storage devices for electric and hybrid vehicles as a trend for replacing internal combustion engine vehicles with electric and hybrid vehicles is increasing to prevent the generation carbon dioxide (CO_2), a major greenhouse gas. They are also used to store the energy generated by intermittent renewable energy sources like solar and wind. The increasing demand for energy storage requires further improvements in the existing Li-ion batteries and the development of next-generation Li-ion batteries, especially to enhance safety and reduce the cost and capacity fading of Li-ion batteries. Figure 1.4 shows the future requirements of Li-ion batteries. To meet the future requirements of Li-ion batteries, researches are being conducted in different aspects

of Li-ion batteries such as liquid electrolytes are being replaced with solid electrolytes [12], different materials are being considered for anode active materials to overcome the drawbacks of graphite [13], [14].

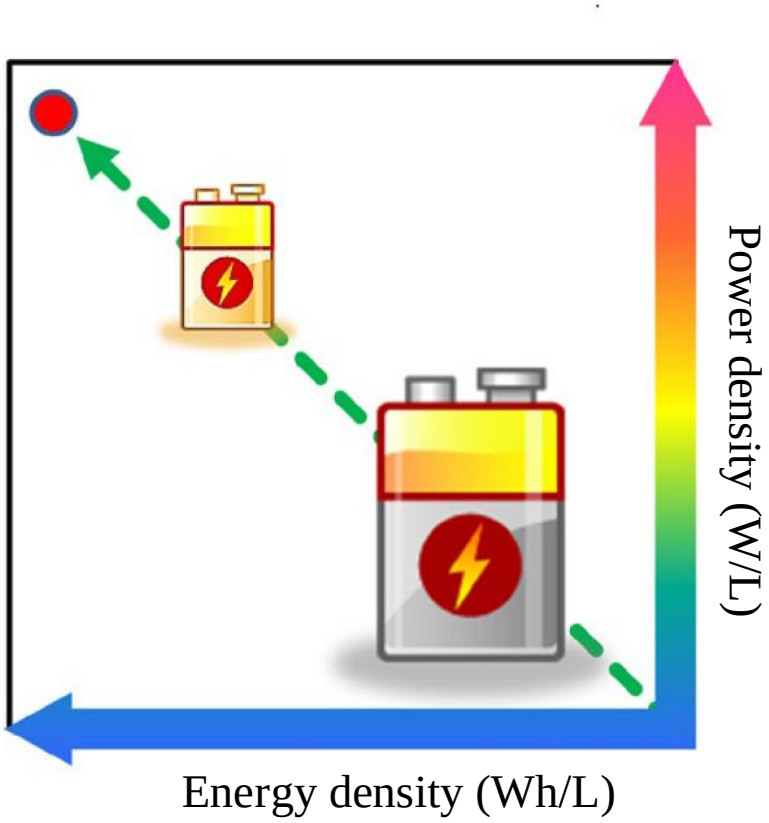

Figure 1.4. The illustration to a demonstration that future Li-ion batteries should be light and small without any compromise on energy and power [11].

1.2 Literature review

Li-ion batteries attracted much more worldwide attention after its commercialization by Sony [15]. The global production of Li-ion batteries has rapidly increased since past two decades. This has been achieved through the active research. Mathematical modeling has played key roles in the design optimization and understanding

the capacity fading mechanisms due to various side reactions.

According to the literature, Equivalent Circuit Models (ECMs) and Electrochemical Models (EMs) are the models used for simulation of Li-ion battery. ECMs uses only electrical components to model the performance of the battery. Generally, there are three variations of ECMs model.

(a) R_{int} model where only a resistance and a voltage source are used to model the battery
(b) RC model where capacitor dynamics have been added to R_{int} model [16]
(c) Thevenin model extension of the RC model.

ECMs are simpler, cheaper and faster, but they have a tendency to fail at various operating conditions leading to inaccurate results [17]. The applications requiring accurate results use EMs models.

In contrast to ECMs, EMs model describes the electrochemical phenomena taking place in the battery through the means of different governing mathematical equations. They are more accurate than ECMs model because of their ability to describe detailed physical phenomena taking place inside the batteries. Pseudo two dimensional (P2D) based on porous electrode theory is the most widely used EMs models [18].

P2D model was first developed by Newman and his co-workers (1993) [19]. This model treats the electrode as a homogeneous electrode continuum [20]. It ignores the microscopic structures in the electrode; however, change in effective properties of electrodes was accounted by use of Bruggeman's equation [21]. This model is further developed and coupled with transport phenomena and electrochemical reaction

engineering. Further, the model has been extended to describe various degradation mechanisms and side reactions occurring within the cell. The full order battery model takes a lot of time to provide the solutions for governing equations. Researchers have reduced the order of the battery model using different approaches. Subramanian *et al.* (2007) [22] reduced the model using a combination of perturbation techniques and heuristic simplifications. They reported that the computational time for their real-time simulation model for a single process to be around 100 ms, but the model required preprocessing and prior knowledge of the behavior of the system under different conditions, which makes their model less flexible. Other methods, including the Chebyshev polynomial method, the residue grouping method, proper orthogonal decomposition method, and Padé approximation, have also been used to derive reduced-order models for Li-ion batteries [23].

As the demand for the higher energy density Li-ion battery increased, a lot of efforts have been made to improve the electrode design. The straightforward design to increase the energy density is to increase the electrode thickness. However, the increased electrode thickness impairs electrolyte-phase mass transfer, thereby making the design unsuitable for desired applications [19], [24], [25]. The electrode thickness depends on the nature of the applications. The high-power applications need thinner electrodes whereas the high energy applications require thicker electrodes [25]. The thickness constraints are serious in Li-ion cells due to the low transport properties of non-aqueous electrolyte [25], [26]. Many studies have shown that the electrolyte limits the use of the battery in discharge applications [27], [28]. To increase the energy density by increasing electrode thickness electrolyte phase limitation should be overcome, which can be achieved through proper

tuning of electrode's porosity and thickness.

Mathematical models are coupled with optimization protocols to predict the optimal porosity and thickness for maximizing the energy density for a given discharge time. Tiedmann and Newman (1975) [24] first illustrated an approach to optimize porous electrodes by using simplified reaction zone model. In this model, they obtained an analytical solution by confining the Li-ion intercalation to a narrow zone in the positive electrode and used solution to get the optimal design. Over the years, Newman and co-workers removed the simplifications and used a generalized model to optimize different battery systems [25], [29]. However, these methods did not make any changes in the commercial batteries mainly due to the lack of manufacturing methods to fabricate thick electrodes.

Subsequently, researchers focused on the variable porosity of electrode. The varying porosity approach is thought to ensure greater access to electrolyte allowing the electrode thickness to increase leading to an increase of the energy density without affecting power capability. Ramadesigan *et al.* (2010) [30] observed 15-30% reduction of electrolyte resistance in varying porosity model compared to constant porosity model. Furthermore, Golman *et al.* (2014) [31] demonstrated improvement of discharge capacity by approximately 30% for a half-cell configuration and by 60% for a full-cell by implementing a varying electrode porosity model. Reduction in the liquid phase resistance is attributed as a reason for increased capacity in the varying electrode porosity model. In these studies, optimized varying porosity designs were compared with arbitrary base designs. The optimization shows improvement in energy density with respect to base design, but cannot guarantee that the sole reason for improvement of capacity is varying

porosity.

Dai *et al.* (2016) [32] developed the battery model based on the macro homogeneous approach and then developed an optimization algorithm to predict optimal values of porosity and thickness to maximize the energy density for a given time of discharge. In their study, they compared optimized constant porosity system with an optimized varying porosity system to validate the advantage of varying porosity design. However, they observed very little improvement using varying porosity design.

Recently, researchers have considered a modification in the design of current collector to improve the performance of the battery. Yao *et al.* (2007) [33] used a three-dimensional substrate as current collector prepared by foamed polyurethane and nickel-chromium alloy and it exhibited approximately three times power than that using a foil-type aluminum current collector. Furthermore, Tian *et al.* (2015) [34] used a 3D carbon nano-network fabricated on scalable manufactured 3D porous anodized alumina templates on 3D C/TiO_2 nano-network electrodes and achieved a large areal capacity of approximately 0.37 mAh cm^{-2}. It also demonstrated a long cycle life over 1000 cycles with a capacity retention of 91%. However, no mathematical governing equations have been reported on porous current collectors in the literature. The dependence of solid electrolyte interphase (SEI) growth and state of health (SOH) has not been well understood in Li-ion battery.

1.3 Motivation

There is a need to adjust the existing governing equations to explain the performance of porous current collector based Li-ion batteries and to compare the capacity fading of

porous current collector based Li-ion batteries with other types of Li-ion batteries.

1.4 Objectives

The purpose of this thesis is to provide a mathematical explanation for improved performance of porous current collector based Li-ion battery and perform the simulation study to compare the capacity fading of porous and non-porous current collector based batteries.

1.5 Contributions

The main contributions of this thesis are stated below:

(a) Generalized P2D model by adjusting the governing equations and boundary conditions for the case of porous current collector based Li-ion batteries.

(b) Determined porosity of porous current collector by applying image processing techniques for experimentally obtained scanning electron microscopy (SEM) image.

(c) Compared capacity fading in porous and non-porous current collectors based Li-ion batteries.

1.6 Thesis outline

This thesis has been organized as follows: Chapter 2 provides the classifications of batteries, lists important battery terminology, explains the operation of Li-ion battery and explains the numerical method to solve the differential equations. Chapter 3 presents the assumptions made for modeling, explains the changes in the governing equations due to use of the porous current collector and describes the capacity fading in Li-ion battery. Chapter 4 explains MATLAB simulation model, describes the method used to determine the porosity and pores distribution of the porous current collector, presents the results for

discharge performance and capacity fading. Lastly, Chapter 5 presents the summary, conclusion, and future works related to this thesis.

CHAPTER 2 THEORY

A battery is an electrochemical device that can be charged electrically to store energy and can be discharged electrically when needed. The energy conversion takes place by means of electrochemical oxidation-reduction reaction. This type of reactions occurs due to the transfer of electrons from one type of materials to another through an electric circuit. A battery consists of anode, cathode, and electrolyte as major components which are defined briefly below.

(a) **Anode**: Anode is also known as a negative electrode which provides electrons to an external circuit and is oxidized during the electrochemical reaction. Anode must be an efficient reducing agent, should have good conductivity stability, high coulombic output, low cost and should be easy to fabricate. Metals are mainly used as anode materials.

(b) **Cathode**: Cathode is also known as a positive electrode which accepts electrons from an external circuit and is reduced during the electrochemical reaction. Cathode must be an efficient oxidizing agent, stable when in contact with the electrolyte and have a useful working voltage. Metal oxides are common cathode materials.

(c) **Electrolyte**: Electrolyte is the ionic conductor which provides a medium for transfer of charge as ions inside the battery between anode and cathode. Typically, the electrolyte is a liquid like water or other solvents with dipped salts, acids or alkalis. The electrolyte should have high ionic conductivity and low electronic conductivity. They should be nonreactive with electrode materials and safe in handling, should have low cost and their properties should not change with variations of temperature.

In practical battery anode and cathode are isolated electronically to avoid internal short-circuiting, but they are surrounded by an electrolyte. Anode and cathode electrodes are separated mechanically by a thin permeable separator. Permeable separator allows electrolyte to pass through which maintains desired ionic conductivity.

2.1 Battery classifications

Based on electrical rechargeability, batteries are classified as primary and secondary batteries.

(a) **Primary battery**: Primary battery is not rechargeable meaning it is designed for one-time use. The electrochemical reaction taking place inside the primary battery is irreversible.

The primary battery has light weight which makes it suitable power source for portable electronic and electric devices like flashlights, toys, memory backup. High capacity primary batteries are useful where charging is impractical such as military combat, rescue missions. The major advantages of the primary battery are a long life, the high energy density at low and moderate discharge rate, little maintenance and ease of use. Safe disposal is the main challenge of the primary batteries.

(b) **Secondary battery**: Secondary battery can be recharged to its original capacity by applying the current in the opposite direction of the discharge current. The electrochemical reaction taking place inside the battery is reversible.

Secondary batteries have high power density, high discharge rate, flat discharge curves, and good low-temperature performance. Their energy densities and charge retention are poor than that of primary batteries. Figure 2.1 compare specific energy

between different types of primary and secondary batteries.

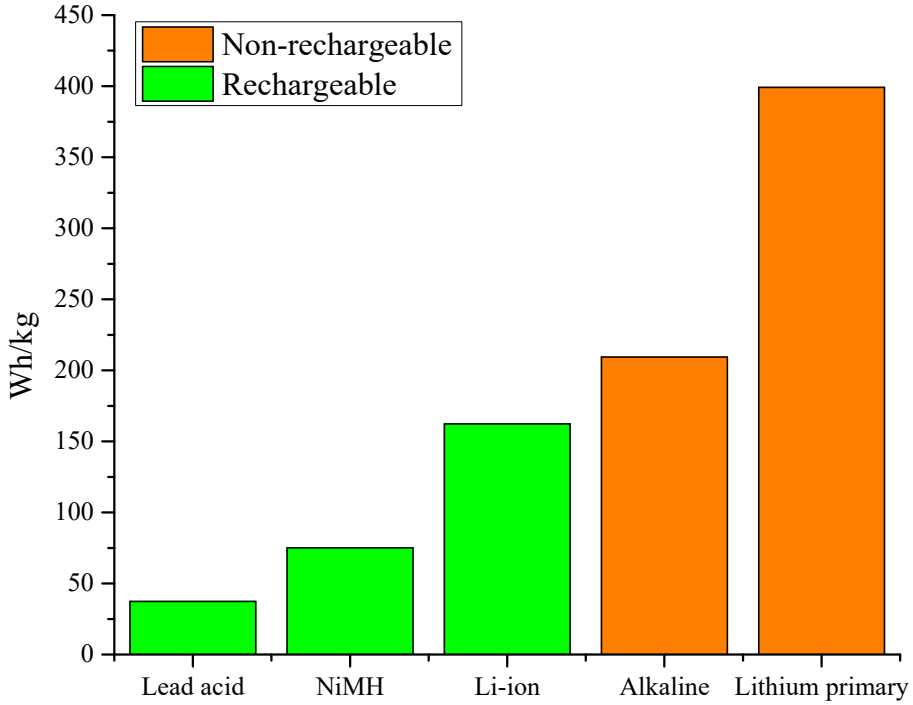

Figure 2.1. Specific energy comparison of secondary and primary batteries [35].

Applications of secondary batteries fall under two categories. First, they are used as energy storage devices, where they are electrically connected and charged by a primary sources like electric grid and supplies energy based on load demand. Hybrid electric vehicles, standby power supply, and aircraft systems are some of the examples. Second, they are discharged like primary batteries and recharged periodically instead of disposal. Electric vehicles, portable electronic devices, power tools are some of the examples in which secondary batteries are discharged in the similar fashion of primary batteries.

2.2 Battery terminology

Battery manufacturer uses certain terminologies to describe, classify and compare the batteries for different applications. These terminologies are important to characterize the battery operating conditions and to understand the manufacturer specifications. The following definitions for battery terminologies are taken from [36].

(a) **C- and E- rates**: A C-rate is a measure of the rate at which a battery is discharged relative to its maximum capacity. A 1C rate means that the discharge current will discharge the battery completely in 1 hour. For 1 Ah battery, the 1C rate is 1 amps for 1 hours, the 2C rate is 2 amps for 30 minutes and the C/2 rate is 0.5 amps for 2 hours. Similarly, an E-rate describes the discharge power. A 1E rate is the discharge power to discharge the battery completely in 1 hour.

(b) **State of charge (SOC) (%)**: The present battery capacity as a percentage of maximum capacity is termed as the state of charge of battery. SOC provides the information on the change in battery capacity over the time.

(c) **Depth of discharge (DOD) (%)**: The battery capacity that has been discharged expressed as a percentage of maximum capacity. The battery capable of at least 80% depth of discharge is termed as deep cycle battery.

(d) **Terminal voltage (V)**: The voltage between two terminals of the battery under the loaded condition is called terminal voltage. Terminal voltage varies with SOC and charge and discharge currents.

(e) **Open-circuit Voltage (V)**: The voltage between terminals of the battery under no load condition is called open-circuit voltage. It increases with state of charge.

(f) **Internal resistance**: The resistance of the battery that is different for charging and discharging. Power loss in the internal resistance is the cause of temperature rise of the battery. Internal resistance increases over the time of use which reduces the battery efficiency and thermal stability.

(g) **Nominal voltage (V)**: The reference or reported voltage of the battery.

(h) **Cut-off voltage (V)**: The minimum allowable voltage that defines the empty state of the battery is called cut-off voltage.

(i) **Capacity or nominal capacity (Ah for a specific C-rate)**: Amp-hours available when the battery is discharged at a certain discharge current (specified as a C-rate) from 100 percent state-of-charge to the cut-off voltage. It is calculated by integrating the current over the period of discharge. It decreases with increasing C-rate.

(j) **Energy or nominal energy (Wh (for a specific C-rate))**: The total Watt-hours available when the battery is discharged at a certain discharge current (specified as a C-rate) from 100 percent state-of-charge to the cut-off voltage. It decreases with increasing C-rate.

(k) **Cycle Life**: The number of discharge-charge cycles after that the battery fails to meet the specific performance criteria is called cycle life. The actual operating life of the battery is affected by the rate and depth of cycles and by other conditions such as temperature and humidity. Discharging battery at higher rate reduces cycle life of the battery.

(l) **Specific energy (Wh/kg)**: The nominal energy of the battery per unit mass is called specific energy. It determines the weight of the battery required to meet the given

electric range.

(m) **Specific power (W/kg)**: Specific power is the maximum power per unit mass. It determines the weight of the battery required to meet the performance target.

(n) **Energy density (Wh/L)**: Energy density also known as volumetric energy density is the nominal energy of the battery per unit volume. It determines the size of the battery required to meet the given electric range.

(o) **Power density (W/L)**: Power density is the maximum power per unit volume. It determines the size of the battery required to meet the performance target.

(p) **Maximum continuous discharge current**: The maximum current at which battery can be discharged continuously. The limit is usually set by the manufacturer in order to prevent the damage of battery by excessive discharge.

(q) **Maximum 30-sec discharge pulse current**: The maximum current at which the battery can be discharged for pulses of up to 30 seconds. The limit is usually set by the manufacturer to prevent the damage of battery by excessive discharge.

(r) **Charge voltage**: The voltage of the battery when it is charged to full capacity is charge voltage. Generally, two-stage charging schemes are in practice. In the first stage, the battery is charged with constant current until the voltage reaches to charge voltage and in the second stage, voltage is maintained at charge voltage by reducing the charging current.

(s) **Float voltage**: The voltage at which battery is maintained after it is charged to 100% SOC to compensate for loss due to self-discharging.

2.3 Rechargeable battery chemistry

Rechargeable batteries play very important role in our day-to-day life. Lead-acid, NiCd, NiMH, and Li-ion are commonly used chemicals in rechargeable batteries. They are briefly explained below. Figure 2.2 summaries the classifications of the battery along with battery chemistries for secondary batteries.

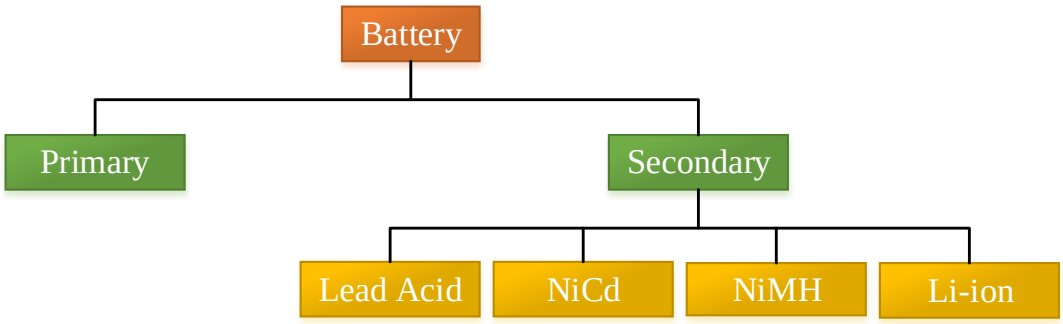

Figure 2.2. Classifications of battery with different chemistries of secondary batteries.

(a) **Lead acid**: Lead-acid is the oldest rechargeable battery system. Lead-acid is rugged and cheap, but it has lower capacity and cycle count. Lead-acid is widely used in wheelchairs, golf cars, personnel carriers, emergency lighting. Due to the toxicity of lead, safe disposal is a major challenge.

(b) **Nickel-cadmium (NiCd)**: For the applications which require long service life, high discharge rates, and extreme temperatures operation NiCd batteries are very useful. Ultra-fast charging with minimum stress is possible with this chemistry. NiCd are widely used in power tools, medical devices, aviation. It is being replaced by other chemistries as cadmium is not environmental friendly.

(c) **Nickel-metal-hydride (NiMH)**: This chemistry act as a replacement of NiCd. It

replaces toxic cadmium (Cd) with mild toxic metal. It has higher specific capacity. Medical instruments, hybrid cars, and industrial applications are the applications where NiMH is used.

(d) **Li-ion**: This battery chemistry is replacing other rechargeable battery chemistries. It is most popular chemistry at present time. It has energy density almost twice that of standard NiCd. Li-ion batteries are maintenance free, have no memory effect, and low self-discharge. However, they are fragile and requires protection circuits for safe operation.

2.4 Basics of Li-ion battery

A basic Li-ion cell consists of an anode, a cathode, an electrolyte and separator as main components. Anode and cathode are contacted by an electrolyte containing Li-ions. The electrolyte may be liquid, polymer, gel or ceramic. Separator usually micro porous polymer membrane isolates electrodes from each other. Separator allows the flow of ions between the two electrodes but prevents electrons flow inside the battery.

The commercial cells are assembled in the discharge state. Discharged anode materials and cathode materials are stable in the atmosphere and safe to handle. During charging, external electrical supply is connected to the two electrodes of the cell. The electron released at cathode moves to anode externally. At the same time, Li-ions move in the same direction of movement of electrons inside the battery through the electrolyte. This phenomenon stores external electrical energy electrochemically in the form of chemical energy in the anode and cathode materials with different chemical potentials. During discharge, the electrons move from anode to cathode through the externally

applied load to do the useful work and Li ions move from anode to cathode through the electrolyte. Figure 2.3 shows major components of Li-ion cell and illustrates the charging and discharging mechanism of Li-ion cell.

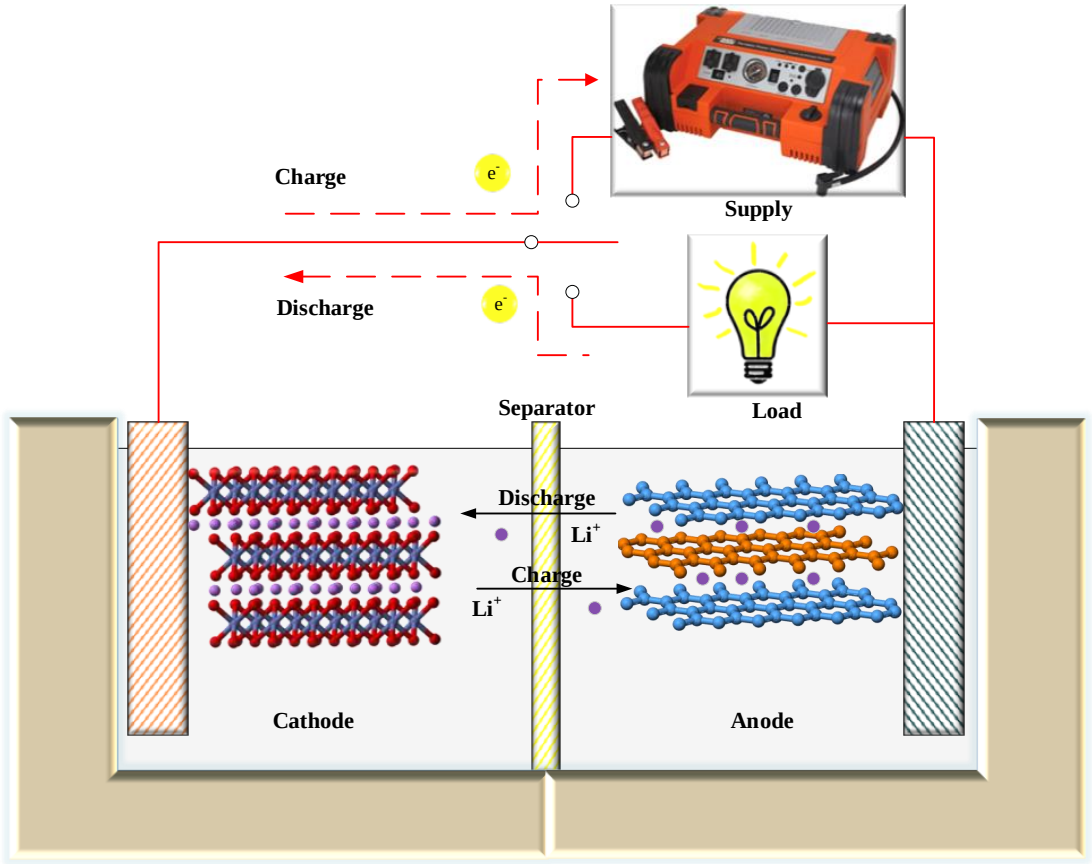

Figure 2.3. The components of a typical Li-ion battery and the electrochemical processes in charging and discharging. The typical cathode and anode materials are $LiCoO_2$ and graphite respectively [37].

The chemical reactions taking place inside the battery during charging and discharging for battery chemistry shown in figure 2.3 are shown below.

At the anode:

$$Li_xC_6 + xLi^+ + xe^- \underset{charge}{\overset{discharge}{\rightleftharpoons}} LiC_6 \tag{2.1}$$

At the cathode:

$$\mathrm{LiCoO_2} \underset{charge}{\overset{discharge}{\rightleftharpoons}} \mathrm{Li_{(1-x)}CoO_2} + \mathrm{xLi^+} + \mathrm{xe^-} \tag{2.2}$$

Overall:

$$\mathrm{Li_xC_6} + \mathrm{LiCoO_2} \underset{charge}{\overset{discharge}{\rightleftharpoons}} \mathrm{LiC_6} + \mathrm{Li_{(1-x)}CoO_2} \tag{2.3}$$

Lithium battery doesn't have fixed chemistry. A number of combinations of cathode and anode materials have been evaluated since the commercialization [38]. Figure 2.4 shows different electrode materials used in Li-ion batteries. Based on the type of cathode or anode material used lithium batteries are classified into different chemistries. The following section provides a brief overview of six famous Li-ion battery chemistries. The explanation is taken from [39].

(a) **Lithium cobalt oxide ($\mathbf{LiCoO_2}$)**: This battery chemistry consists of cobalt oxide cathode and a graphite carbon anode. It is suitable for portable electronic devices like mobile phones, laptops, and a digital camera because of its high specific energy. It has short cycle life, low thermal stability, and limited load capabilities. This chemistry is not suitable for the applications requiring charging and discharging above C-rating.

(b) **Lithium manganese oxide ($\mathbf{LiMn_2O_4}$)**: This chemistry uses manganese oxide as the cathode material. The three-dimensional spinel structure of manganese oxide improves lowers internal resistance and improves current handling capability by

improving the ion flow on the electrode. It has high thermal stability and better safety, but the cycle life is limited. It can be charged and discharged above C-rating.

(c) **Lithium nickel manganese cobalt oxide (NMC)**: Cathode is formed by the combination of nickel, manganese, and cobalt. Nickel has high specific energy and poor stability whereas manganese lowers internal resistance through spinel structure and has lower specific energy. The combination of nickel and manganese compliments to each other. This chemistry is suitable for power tools, e-bikes, and other electric power trains.

(d) **Lithium iron phosphate ($LiFePO_4$)**: Lithium iron phosphate as cathode material was discovered by the University of Texas in 1996. It has good thermal stability, high current rating and long cycle life. It has lower specific energy compared to lithium cobalt oxide and other mixed metal oxide chemistries because of its lower nominal voltage of 3.2V/cell. Cold temperatures degrade performance and elevated temperatures reduce cycle life.

(e) **Lithium nickel cobalt aluminum oxide ($LiNiCoAlO_2$)**: This chemistry offers high specific energy and specific power. It has a long life. It is cheaper and safer than the lithium cobalt oxide based battery.

(f) **Lithium titanate ($Li_4Ti_5O_{12}$)**: Li-titanate replaces the graphite in the anode of a typical Li-ion battery and the material forms into a spinel structure. The cathode can be $LiCoO_2$, $LiFePO_4$ or NMC. It can be charged fast and can discharge at the rate 10 times the rated C-rating. It is safe, has long cycle life, excellent low temperature discharge performance. However, it has low specific energy and is expensive.

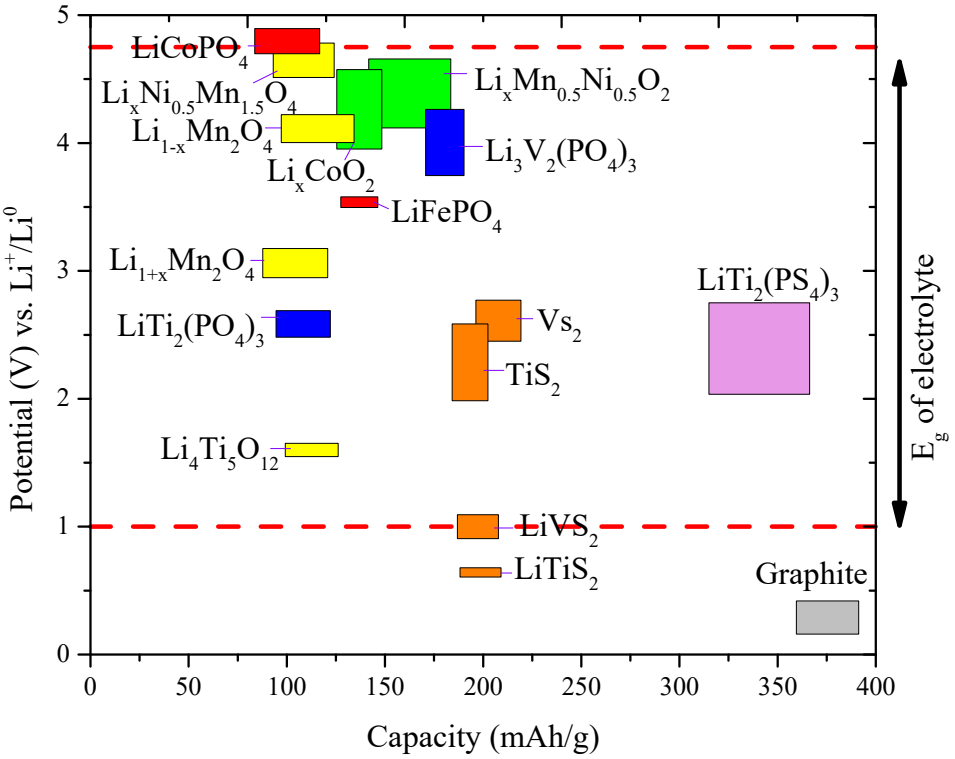

Figure 2.4. Different electrode materials for Li-ion batteries [40].

2.5 Capacity fading

The amount of charge that a battery can deliver at rated voltage decreases with the time of use and this phenomenon is known as capacity fading or capacity loss. This phenomenon takes place regardless either battery is ideal or in use [41]. There are two types of capacity loss: reversible and irreversible. The reversible capacity loss is due to self-discharging of battery and it can be recovered by charging the battery. The irreversible loss is due to degradation of battery and this loss cannot be recovered.

The degradation of the battery occurs due to many complicated phenomena and side reactions taking place simultaneously at various places of the battery [42]. The rate of degradation depends on the rate of discharge, temperature, and cell materials

combinations. Some of the side reactions taking place inside the battery are passive film formation, electrolyte decomposition, gas evolution and active materials decomposition [43], [44]. These unwanted reactions consume active material and electrolytes leading to the formation of insoluble solid, some liquid and gaseous products. Electrolyte decomposition leads to the formation of the passive layer at anode known as a solid-electrolyte interface (SEI) [45]. SEI thickness increases over the charging cycle and causes the voltage loss and increase the internal resistance of the battery and hence results in an irreversible capacity loss.

The typical range of capacity loss in the Li-ion battery after 500 charging and discharging cycle varies from 12.4% to 24.1%, resulting in an average capacity loss per cycle in the range of 0.025–0.048% per cycle [41].

2.6 Current collectors

Typically, copper and aluminum are used as anode and cathode current collectors respectively in the conventional Li-ion battery. Current collectors play important role in the operation of the battery. The chemical and physical properties of current collectors can affect the performance of the battery [46]. The role of current collectors is to transfer the charge efficiently to active materials of the electrode. Researchers are modifying the structure of current collectors to increase the charge transfer efficiency. In this work, the porous current collector is considered an anode current collector. Use of porous current collector is believed to increase specific surface area, electronic conductivity and reduce the insignificant mass of the battery.

2.7 Numerical method

First principle battery model consists of non-linear coupled partial differential equations(PDEs). These partial differential equations can be solved analytically or by numerical methods. Although analytical solutions are accurate, all PDEs cannot be solved analytically. Numerical approximation methods are used to solve PDEs those cannot be solved analytically. In numerical methods, partial differential equations are discretized and represented by difference equations. Finite element, finite volume, finite difference methods are some of the numerical methods to solve the partial differential equations. In this work, finite difference method is used to solve the partial differential equations involved in battery model.

2.7.1 Finite difference method (FDM)

The finite difference is discretization method to solve the differential equations in which differential equations are approximated by difference equations. Finite difference approximates the derivatives. This method is one of the simplest and oldest methods to solve the differential equations by numerical approximations. The details and examples of finite difference methods can be found in [47].

In the finite difference method, independent variable of PDE is defined by a finite grid or mesh and at each grid points value of the dependent variable is approximated. The approximation is done by using of Taylor's theorem. The difference may be the forward difference, backward difference or central difference depending on whether the data on future, past or both used to approximate the derivatives. The following section shows the finite difference approximation of first derivative $\frac{du}{dx}$ and second derivative $\frac{d^2u}{dx^2}$ by forward,

backward and central difference.

Forward difference:

$$\begin{aligned} \frac{du}{dx} &\approx \frac{u(x+h)-u(x)}{\Delta x} \\ \frac{d^2u}{dx^2} &\approx \frac{u(x+2h)-2u(x+h)+u(x)}{\Delta x^2} \end{aligned} \tag{2.4}$$

Backward difference:

$$\begin{aligned} \frac{du}{dx} &\approx \frac{u(x)-u(x-h)}{\Delta x} \\ \frac{d^2u}{dx^2} &\approx \frac{u(x)-2u(x-h)+u(x-2h)}{\Delta x^2} \end{aligned} \tag{2.5}$$

Central Difference:

$$\begin{aligned} \frac{du}{dx} &\approx \frac{u(x+h)-u(x-h)}{2\Delta x} \\ \frac{d^2u}{dx^2} &\approx \frac{u(x+h)-2u(x)+u(x-h)}{\Delta x^2} \end{aligned} \tag{2.6}$$

For solving time-dependent differential equation, FDM may be an explicit or implicit method. A finite difference scheme is said to be explicit if the solution at a future time is computed using the solution of the current time and it is said to be implicit if a solution is found by solving an equation involving future value and current value. Explicit method is simple to solve and has the less computational burden, but need smaller time steps for accuracy and stability. Implicit methods are computationally intensive but are always stable and convergent.

If $Y(t)$ is the state at current time and $Y(t+\Delta t)$ is the state in future time, $Y(t+\Delta t)$ by explicit method is computed using the equation,

$$Y(t+\Delta t) = F(Y(t)) \tag{2.7}$$

In implicit method following equation is solved to find the $Y(t+\Delta t)$

$$F(Y(t), Y(t+\Delta t)) = 0 \tag{2.8}$$

CHAPTER 3 BATTERY MODELING

Equivalent circuit and electrochemical modeling are two commonly used battery modeling approaches. In equivalent circuit battery model, electrochemical physics of battery are modeled using electrical components. The advantage of equivalent circuit model is that it is easier and simpler to implement; however, it is less accurate. In electrochemical battery modeling, the battery physics are described by using non-linear partial differential equations. The electrochemical battery model requires high computational time, but they predict accurate results compare to equivalent circuit model. In this work, electrochemical battery model is considered.

A pseudo-two-dimensional (P2D) model based on the porous electrode and concentrated theory proposed by Newman and Tiedmann [48] and Doyle *et al.* (1993) [19]. This model mathematically describes charge/discharge and species transport in the solid and electrolyte phases across a simplified 1D spatial cell structure using porous current collector. As an anode is limiting electrode [49] in the Li-ion battery, the porous current collector is considered at limiting electrode side. Figure 3.1 shows the schematic of the battery considered for modeling.

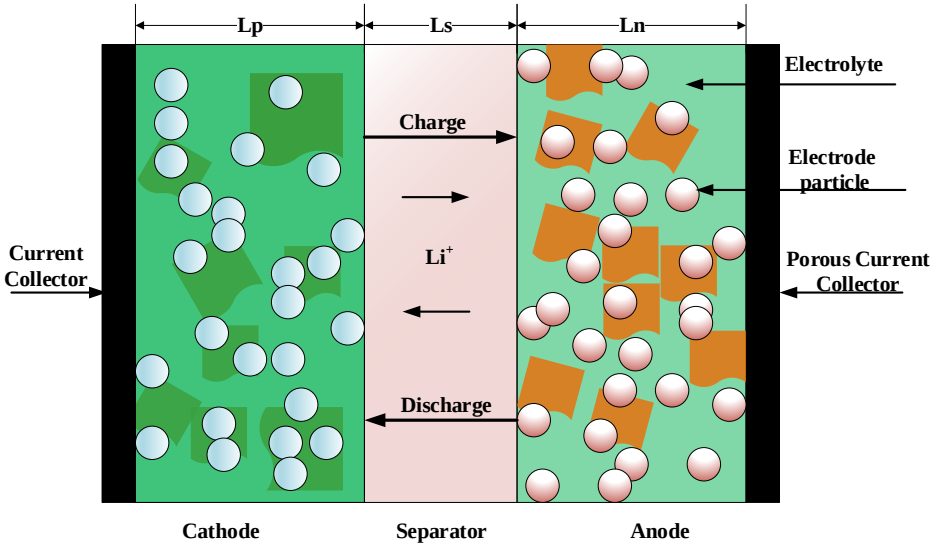

Figure 3.1. Schematic of Li-ion battery.

3.1 Model assumptions

For simplifying the modeling problem certain assumptions were made. Electrode particles are assumed to be spherical in shape. The pores on the current collector are assumed to be uniform and the diameter of the pores is assumed to fit the spherical electrode particles. The electrolyte can penetrate to the pores of current collector through the pores of the electrode. The depth of the current collector's pores is not considered in governing mathematical equations. Non-porous part of the current collector at electrode current collector interface is taken as a boundary for adjusting the governing equations. Figure 3.2 graphically shows the assumptions made to adjust the battery model for the case of the porous current collector.

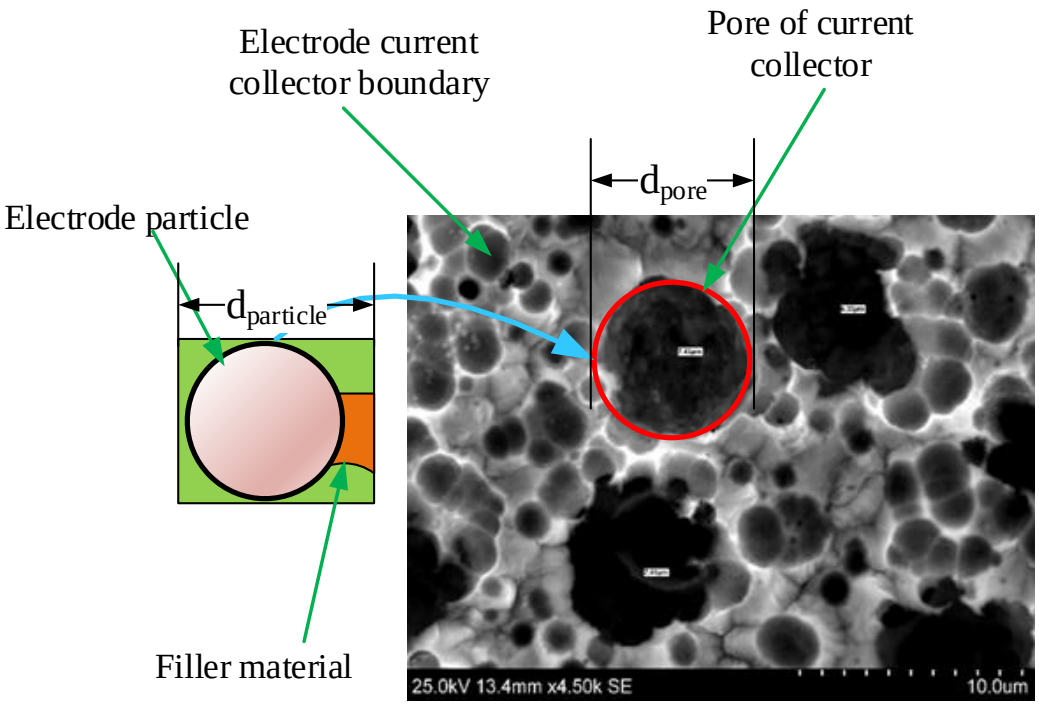

Figure 3.2. SEM image of porous copper and graphical illustration of model assumptions. SEM image is taken from [50].

3.2 Battery model

The notable change observed by using porous current collector is the volume fraction of the electrode material, which affects the effective electronic conductivity, specific surface area, electrodes masses and other governing equations and boundary conditions.

The volume fraction of electrode active material is $(1-\varepsilon_k-\varepsilon_{f,k})$, where ε_k and $\varepsilon_{f,k}$ are electrode porosity and filler material volume fraction. If ε_{cc} is the porosity of current collector, the electrode active materials will be occupying the ε_{cc} portion of the current collector. The volume fraction of the electrode material in the current collector is $\varepsilon_{cc}(1-\varepsilon_k-\varepsilon_{f,k})$. Thus, net volume fraction with the use of porous current collector is

$(1-\varepsilon_k-\varepsilon_{f,k})+\varepsilon_{cc}(1-\varepsilon_k-\varepsilon_{f,k})$, which is equal to $(1-\varepsilon_k-\varepsilon_{f,k})(1+\varepsilon_{cc})$.

The effective electronic conductivity σ_{eff} and specific surface area a_k of the electrode depend on the volume fraction of electrode active materials. The effective electronic conductivity is given by Bruggeman equation as,

$$\sigma_{eff,k} = \sigma_k(1-\varepsilon_k-\varepsilon_{f,k}) \tag{3.1}$$

$$\sigma_{eff,k} = \sigma_k(1-\varepsilon_k-\varepsilon_{f,k})(1+\varepsilon_{cc}) \tag{3.2}$$

Equation 3.1 and equation 3.2 are the expressions for the effective electronic conductivity of electrode for with foil type and porous current collectors respectively. From these equations, it can be inferred that the effective electronic conductivity is higher for the case of porous current collectors. The specific electrode surface area is expressed as,

$$a_k = \frac{3}{R_P}(1-\varepsilon_k-\varepsilon_{f,k}) \tag{3.3}$$

$$a_k = \frac{3}{R_P}(1-\varepsilon_k-\varepsilon_{f,k})(1+\varepsilon_{cc}) \tag{3.4}$$

where R_P is radius of spherical particle. Equation 3.3 and equation 3.4 are the expressions for the specific surface area for non-porous and porous current collectors. From these equations, the specific surface area of the electrode is higher for the case of the porous current collector.

According to porous electrode theory, lithium exists in two disjoint states called phases. Lithium is in solid phase in electrode material and in liquid phase state in electrolyte.

3.2.1 Transport in solid phase

According to Fick's laws of diffusion, the solid phase Li^+ concentration c_s in a single spherical active material particle can be described as,

$$\frac{\partial c_s(r,t)}{\partial t} = \frac{D_{s,k}}{r^2}\frac{\partial}{\partial t}\left[r^2\frac{\partial c_s(r,t)}{\partial r}\right] \tag{3.5}$$

with boundary conditions

$$-D_{s,k}\frac{\partial c_{s,k}}{\partial r}\bigg|_{r=0} = 0 \tag{3.6}$$

$$-D_{s,k}\frac{\partial c_{s,k}}{\partial r}\bigg|_{r=R_P} = J_k(x,t) \tag{3.7}$$

where r is the radial direction along which the ions intercalate within the electrode particles, D_s is solid phase diffusion coefficeint, J_k is wall flux of Li^+ on intercalation particle of electrode, $k = p$ for the positive electrode and $k = n$ for the negative electrode. Definitions of symbols are given in nomenclature section. In this model r is a pseudo-second dimension. Two-term polynomial approximation method is used to reduce the complexity and computational burden. This method is accurate for low to medium C rates [51].

In two-term polynomial approximation, equation 3.5 is approximated by means of

average $c_{s,k}^{avg}$ and surface concentration $c_{s,k}^{*}$ of the solid particles,

$$\frac{\partial c_{s,k}^{avg}(x,t)}{\partial t} = -3\frac{J_k(x,t)}{R_P} \tag{3.8}$$

$$c_{s,k}^{*}(x,t) - c_{s,k}^{avg}(x,t) = -\frac{R_P}{D_{s,k}}\frac{J_k(x,t)}{5} \tag{3.9}$$

Use of two-term polynomial converts the pseudo-two-dimensional problem into one dimensional problem in x. This approximation is not recommended for high C-rates, short time responses or pulse currents as prediction accuracy is predicted to be decreased [51]. For high currents, short-time responses or pulse currents Fick's law and higher-order polynomials are recommended.

3.2.2 Transport in electrolyte

The changes in the gradient diffusive flow of Li^+ ions change the Li^+ concentration $c_{e,k}$ in electrolyte phase. This phenomenon can be explained by following equation,

$$\varepsilon_k \frac{\partial c_{e,k}(x,t)}{\partial t} = \frac{\partial}{\partial x}\left[D_{eff,k}\frac{\partial c_{e,k}(x,t)}{\partial x}\right] + a_k(1-t_+)J_k(x,t) \tag{3.10}$$

The effective diffusion coefficient $D_{eff,k}$ is computed using the Bruggeman equation,

$$D_{eff,k} = D\varepsilon_k^{brugg_k} \tag{3.11}$$

Bruggman's equation considers tortuous path followed by the ions in the porous media.

At the current collectors, the fluxes of ions are zero for all time. This fact is reflected by the boundary conditions of equation 3.10.

At current collectors:

$$-D_{eff,p}\frac{\partial c_{e,p}}{\partial x}\bigg|_{x=0} = -D_{eff,n}(1-\varepsilon_{cc})\frac{\partial c_{e,n}}{\partial x}\bigg|_{x=L} = 0 \tag{3.12}$$

In equation 3.12 for boundary condition at anode, the multiplication factor $(1-\varepsilon_{cc})$ is used to reflect that only the non-porous part of the copper acts as the current collector.

Additional four boundaries exist at the electrode-separator interface. These boundary conditions are based on the continuity of the flux and concentration of the electrolyte at the electrode-separator interface,

$$\begin{aligned}
-D_{eff,p}\frac{\partial c_{e,p}}{\partial x}\bigg|_{x=L_p^-} &= -D_{eff,sep}\frac{\partial c_{e,sep}}{\partial x}\bigg|_{x=L_p^+} \\
-D_{eff,sep}\frac{\partial c_{e,sep}}{\partial x}\bigg|_{x=(L_p+L_{sep})^-} &= -D_{eff,n}\frac{\partial c_{e,n}}{\partial x}\bigg|_{x=(L_p+L_{sep})^+} \\
c_{e,p}\big|_{x=Lp^-} &= c_{e,sep}\big|_{x=Lp^+} \\
c_{e,sep}\big|_{x=(Lp+L_{sep})^+} &= c_{e,n}\big|_{x=(Lp+L_{sep})^+}
\end{aligned} \tag{3.13}$$

3.2.3 Electrical potentials

Electrical potentials are divided into solid phase and liquid phase potentials.

3.2.3.1 Solid phase potential

The potential $\phi_{s,k}$ in the solid phase is explained by Ohm's law,

$$\sigma_{eff,k}\frac{\partial^2\phi_{s,k}(x,t)}{\partial x^2} = a_k F J_k(x,t) \tag{3.14}$$

At the current collector electrode interface, the entire current is carried by the solid phase. The boundary conditions at the current collectors are,

$$-\sigma_{eff,p}\frac{\partial \phi_{s,p}}{\partial x}\bigg|_{x=0} = -\sigma_{eff,n}(1-\varepsilon_{cc})\frac{\partial \phi_{s,n}}{\partial x}\bigg|_{x=L} = I \tag{3.15}$$

where I is current density defined as the ratio of applied current i and the surface area A of the electrode that is $I = i/A$. At separator electrode interface the current is due to the liquid phase. Thus, the solid phase electrode-separator interface current is zero and the boundary conditions at electrode-separator interface are,

$$-\sigma_{eff,p}\frac{\partial \phi_{s,p}}{\partial x}\bigg|_{x=L_p} = -\sigma_{eff,n}\frac{\partial \phi_{s,n}}{\partial x}\bigg|_{x=L_p+L_{sep}} \tag{3.16}$$

3.2.3.2 Liquid phase potential

The liquid phase potential $\phi_{e,k}$ is computed by the application of Kirchhoff's law,

$$\kappa_{eff,k}\frac{\partial \phi_{e,k}(x,t)}{\partial x} + 2\frac{\kappa_{eff,k}(x,t)RT}{F}(1-t_+)\frac{\partial lnc_{e,k}}{\partial x} = -I \tag{3.17}$$

where the ionic conductivity κ_k as a function of electrolyte concentration C_e can be written as,

$$\kappa_k = 0.0158C_{e,k}\exp\left(0.85C_{e,k}^{1.4}\right) \tag{3.18}$$

and the effective ionic conductivity is computed using Bruggeman's equation as,

$$\kappa_{eff,k} = \kappa_k \varepsilon_k^{brugg_k} \tag{3.19}$$

At electrode, current collector interfaces the entire current is carried by solid phase and the liquid phase current is zero. The boundary conditions at electrode current collectors interface are,

$$-\kappa_{eff,p}\frac{\partial \phi_{e,p}}{\partial x}\bigg|_{x=0} = -\kappa_{eff,n}(1-\varepsilon_{cc})\frac{\partial \phi_{e,n}}{\partial x}\bigg|_{x=L} = 0 \tag{3.20}$$

At electrode-separator interface the liquid phase current is continuous. The boundary conditions at the electrode separator interface are obtained by the continuity of $\phi_{e,k}$,

$$-\kappa_{eff,p}\frac{\partial \phi_{e,p}}{\partial x}\bigg|_{x=L_p^-} = -\kappa_{eff,sep}\frac{\partial \phi_{e,sep}}{\partial x}\bigg|_{x=L_p^+} \tag{3.21}$$

$$-\kappa_{eff,sep}\frac{\partial \phi_{e,sep}}{\partial x}\bigg|_{x=(L_p+L_{sep})^-} = -\kappa_{eff,n}\frac{\partial \phi_{e,n}}{\partial x}\bigg|_{x=(L_p+L_{sep})^+} \tag{3.22}$$

3.2.4 Butler-Volmer kinetics equations:

The molar flux $J_k(x,t)$ is calculated using Butler-Volmer kinetics as,

$$J_k(x,t) = a_k J_o\left[\exp\left(\frac{\alpha_a F}{RT}\eta_{s,k}(x,t)\right) - \exp\left(\frac{\alpha_c F}{RT}\eta_{s,k}(x,t)\right)\right] \tag{3.23}$$

The overpotential η which is responsible for driving electrochemical reactions is difference between the battery's electromotive force (EMF) and its charge/discharge voltage. The overpotential is calculated as,

$$\eta_{s,k}(x,t) = \phi_{s,k}(x,t) - \phi_{s,k}(x,t) - U_k(\theta_k(x,t)) - \frac{J_{total}}{a_k}G_{film} \tag{3.24}$$

where J_{total} is total volumetric current density . The dimensionless concentration θ_k is given by,

$$\theta_k(x,t) = \frac{c^*_{s,k}(x,t)}{c_{s,k,max}} \tag{3.25}$$

The constant J_o depends on the concentration $c_{s,k}$ of Li^+ in electrode k and the concentration in the electrolyte as in the following equations,

$$J_o = K_k(c_{s,k,max} - c^*_{s,k})^{\alpha_a}(c^*_{s,k})^{\alpha_a} c^{\alpha_c}_{e,k}(x,t) \tag{3.26}$$

3.2.5 Cell terminal potential

The cell potential $V_{cell}(t)$ is given by,

$$V_{cell}(t) = \phi_{s,p}(0,t) - \phi_{s,n}(L,t) \tag{3.27}$$

Equation 3.27 requires solving two sets of time dependent differential algebraic equations (DAEs). The solution can be obtained numerically using the known initial conditions.

3.3 Reduced order Lithium-ion battery model

Full order battery model is of high order and complexity [52]–[54]. The full battery model is very important because it can be characterized by experimental data and can be used as a benchmark to obtain the reduced order models. Order reduction of battery model provides the opportunity to implement the model into a real-time on-board electronic control unit although they cannot predict current-voltage behavior accurately under

different operating conditions due to approximations of some dynamics of batteries. The main objective of order reduction is to achieve maximum reduction of computational cost while ensuring accurate performance. According to the literature [55], Electrode Averaged Model (EAM) [56] and State Values Model (SVM) [57] are widely used reduced order model.

The EAM model depends on few parameters and it is very simple to set-up whereas SVM model depends on a big number of parameters and is difficult to set up correctly. In this work, EAM model is considered.

3.3.1 Electrode average model (EAM)

The EAM model neglects the solid concentration along the electrode and considers the material diffusion inside a solid particle for each electrode. This approximation leads to an average value of solid concentration that can be related to the definition of battery state of charge and critical surface concentration [58].

The spatial dependence of the Butler-Volmer current is ignored and a constant value $\bar{J}^{Li}$ is considered which satisfies the following spatial integral,

$$\int_0^{L_k} J^{Li}(x)dx = \frac{i}{A} = \bar{J}^{Li}L_k \tag{3.28}$$

where average exchange current density $\bar{J}^{Li}$ is calculated as,

$$\bar{J}^{Li} = \frac{i}{AL_k} = a_k J_o \left[\exp\left(\frac{\alpha_a F}{RT}\bar{\eta}_k\right) - \exp\left(\frac{-\alpha_c F}{RT}\bar{\eta}_k\right)\right] \tag{3.29}$$

$\bar{\eta}_k$ can be calculated as,

$$\begin{aligned} \bar{\eta}_k &= \frac{RT}{\alpha_a F} ln\left(\xi_k + \sqrt{\xi_k^2 + 1}\right) \\ \xi_k &= \frac{\bar{J}^{Li}}{2a_n J_o} \end{aligned} \tag{3.30}$$

The terminal battery voltage can be expressed as a function of battery current and of the solid phase concentration as,

$$V(t) = \frac{RT}{\alpha_a F} ln \frac{\xi_n + \sqrt{\xi_n^2 + 1}}{\xi_p + \sqrt{\xi_p^2 + 1}} + \bar{\phi}_{e,p} - \bar{\phi}_{e,n} + U_p(\bar{C}_{se,p}) - U_n(\bar{C}_{se,n}) - R_{film} I \tag{3.31}$$

where the difference of average electrolyte phase potential $\bar{\phi}_{e,p} - \bar{\phi}_{e,n}$ between the electrodes is calculated as,

$$\bar{\phi}_{e,p} - \bar{\phi}_{e,n} = \phi_e(L) - \phi_e(0) = \frac{-i}{2A}\left(\frac{L_n}{\kappa_n^{eff}} + 2\frac{L_{sep}}{\kappa_{sep}^{eff}} + \frac{L_p}{\kappa_p^{eff}}\right) \tag{3.32}$$

In electrode average model, battery terminal voltage depends on surface charge concentration $C_{s,e}$ through equilibrium potentials U_p and U_n. The equilibrium potentials U_p and U_n depend on surface charge concentration through the state of charge SOC. The state of charge SOC as a function of surface charge concentration is expressed as,

$$SOC = \frac{\theta - \theta_{max}}{\theta_{max} - \theta_{min}} \tag{3.33}$$

where θ can be calculated using equation 3.25, θ_{max} is the ratio of initial surface charge concentration $C_{s,e,init}$ to the maximum solid phase lithium concentration $C_{s,max}$ and the

θ_{min} can be calculated from θ_{max} and battery capacity $Q(Ah)$ as,

$$\theta_{min} = \theta_{max} - \frac{Q}{L_n} \frac{1}{AF\varepsilon_{s,k}C_{s,max}} \tag{3.34}$$

3.4 Capacity fading model

When the Li-ions move from one electrode to another electrode various side-reactions take place, some of which are electrolyte decomposition, passive film formation, gas evolution and active material dissolution. These phenomena lead to capacity fading of the battery which limits the life of the battery.

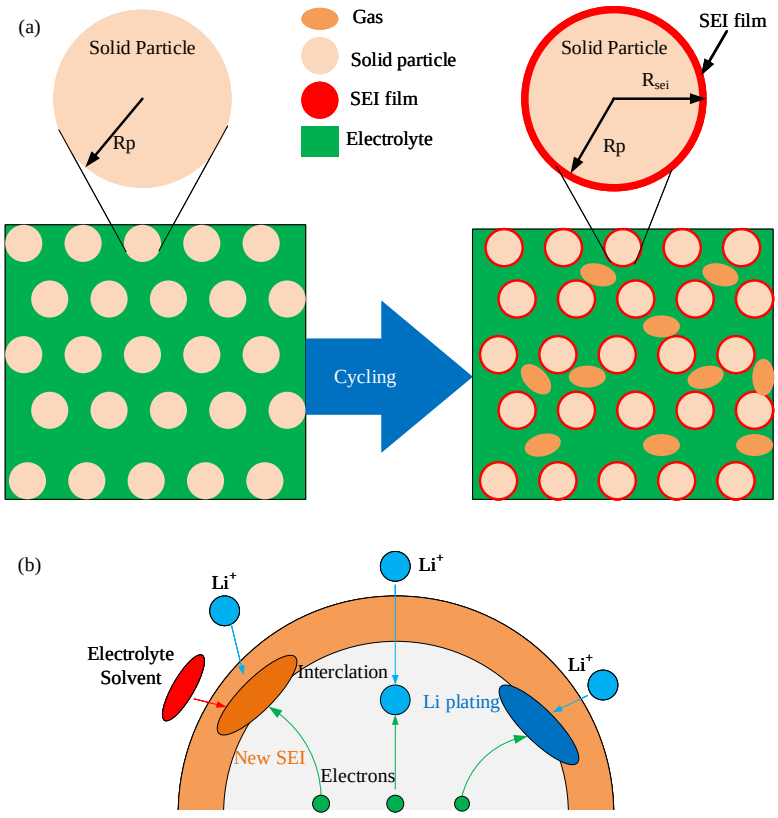

Figure 3.3. (a) Schematic representation of anode before and after cycling [59] and (b) schematic illustration of the electrochemical reactions occurring in the anode during cell charging [60].

Figure 3.3 (a) shows changes taking place on the anode due to cycling and (b) shows different electrochemical reactions taking place during the charging of cell. Generally, three electrochemical reactions can occur in the anode. The main reaction is lithium intercalation reaction and both SEI growth and lithium plating are side reactions. The formation of new SEI at anode surface due to the reaction of lithium with solvent molecule leads to the growth of SEI. In this work gas evolution in anode due to cycling is not considered.

Capacity fade can be split into three components which are a loss in capacity due to increase in resistance at electrodes, loss of lithiation capacity and loss of active material in the cell [49]. Ramadass *et al.* [49] quantify the capacity fade of battery by studying the change in state of charge, film resistance, and diffusion coefficient. The state of charge of the limiting electrode accounts for the capacity loss due to active materials loss, the solid phase diffusion coefficient of the limiting electrode accounts for capacity loss due to rate capability and film resistance accounts for the increase in the polarization and charge transfer resistance with cycling.

3.4.1 Side reactions

Solid electrolyte interface and lithium plating are mainly considered side reactions for capacity fading modeling of Li-ion batteries. During cycling layer forms between anode and electrolyte. This layer is known as a solid-electrolyte interface (SEI). The initial SEI layer acts as a protective layer against large voltage by blocking electron transfer through it while allowing ions to pass. The SEI is a very complex layer composed of inorganic components which are basically salt degradation products and organic

products formed due to the complete or partial reduction of the solvent of the electrolyte [61]. The SEI layer gradually thickens during repeated charge-discharge cycles due to electron exposure to electrolyte or electrolyte diffusion to the anode surface [62]. The continuous growth of the SEI thickness consumes more Li-ions, solvents, and salts. This gradual growth increases the cell resistance and reduces cell capacity.

Deposition of lithium onto the surface of anode particles take place instead of intercalation if the anode potential becomes negative with respect to Li/Li^+ [63]. The plated lithium can form new SEI by reacting with electrolyte or can remain isolated from the electron-conductive matrix, causing loss of lithium inventory. The plated lithium can also induce internal short circuit and result in hazardous consequences.

The surface film covering the anode particles is considered as a mixture of SEI and lithium metal if lithium plating occurs if not, the surface film contains SEI only [60].

The rate of the surface film increase over a cycle is proportional to the current density of SEI formation J_{side} and transfer current density of lithium deposition J_{lpl},

$$\frac{\partial \delta_{film}}{\partial t} = -\frac{J_{side} M_{SEI}}{a_n \rho_{SEI} F} - \frac{J_{lpl} M_{Li}}{a_n \rho_{Li} F} \tag{3.35}$$

where M and ρ are molecular weight and density.

The current density of SEI formation J_{side} is calculated using the cathodic Tafel equation,

$$J_{side} = -a_n i_{os} \exp\left(-\alpha_c f \eta_{side}\right) \tag{3.36}$$

η_{side} is overpotential for side reaction defined as,

$$\eta_{side} = \phi_s - \phi_e - U_{ref,side} - J_{total}\frac{G_{film}}{a_n} \tag{3.37}$$

where $U_{ref,side}$ is equilibrium potential of side reactions.

The total volumetric current density J_{total} is the sum of the intercalation current density J_n, current density of SEI formation J_{side} and current density of lithium deposition J_{lpl}.

$$J_{total} = J_n + J_s + J_{lpl} \tag{3.38}$$

where intercalation current density J_n is calculated using the Butler-Volmer equation 3.23 and the current density of lithium deposition is calculated as,

$$J_{lpl} = -a_n i_{o,lpl} \exp\left[-\frac{\alpha_c F}{RT}\left(\phi_s - \phi_e - \frac{J_{total}}{a_n}G_{film}\right)\right] \tag{3.39}$$

where $i_{o,lpl}$ is the exchange current density of Li deposition. From equations 3.24 and 3.39 the expression for Lithium deposition can be simplified as,

$$J_{lpl} = -a_n i_{o,lpl} \exp\left[-\frac{\alpha_c F}{RT}\left(\eta_n + U_{ref,n}\right)\right] \tag{3.40}$$

Assuming intercalation current density and the side-reaction current densities to be uniform, total volumetric current density J_{total} can be expressed in term of applied current

density I as,

$$J_{total} = -\frac{I}{L_n} \tag{3.41}$$

From equations 3.38 and 3.41, the intercalation current density J_n can be expressed as,

$$J_n = -\frac{I}{L_n} - J_{side} - J_{lpl} \tag{3.42}$$

The SEI formation overpotential η_{side} can be expressed in terms of intercalation overpotential η_n and equilibrium potentials $U_{ref,n}$ and $U_{ref,side}$ as,

$$\eta_{side} = \eta_n + U_{ref,n} - U_{ref,side} \tag{3.43}$$

where intercalation overpotential η_n can be calculated as,

$$\eta_n = \frac{2RT}{F} asinh\left(\frac{J_n}{2a_n J_o}\right) \tag{3.44}$$

Using equaitons 3.43 and 3.44 without considering lithium plating, literature [64] has developed the iterative equation to calculate the SEI formation current density J_{side} assuming J_{side} remains constant over small-time interval Δt. The iterative equation to calculate the SEI formation current density J_{side} with lithium plating consideration is expressed as,

$$J_{side} = -a_n i_{o,s} \exp\left[-\frac{F\left(U_{ref,n} - U_{ref,side}\right)}{2RT}\right] \times \exp\left[-asinh\left(\frac{-I - J_{side} - J_{lpl}}{2a_n J_o}\right)\right] \tag{3.45}$$

.

For each cycle, the thickness increases over time according to

$$\delta_{film}|_N = \delta_{film}|_{N-1} + \delta_{film}(t) \tag{3.46}$$

The film thickness keeps increasing over charge cycles and the overall resistance G_{film} at any cycle is calculated as,

$$G_{film} = \Omega_{SEI} + \frac{\delta_{film}}{\kappa_{SEI}} \tag{3.47}$$

where Ω_{SEI} is initial film resistance.

3.4.2 Effect of side reactions on degradation processes

Loss of anode active material, loss of electrolyte, loss of lithium, the growth of film are the degradation processes caused by side reactions. Above section explains the growth of the film.

The volume fractions of SEI ε_{SEI}, the volume of SEI in a unit volume of composite anode, is expressed in term of current density of SEI formation as,

$$\Delta\varepsilon_{SEI} = \frac{M_{SEI}}{n_{side}F}\int_0^t J_{side}dt \tag{3.48}$$

where n_{side} is the number of electrons involved in the side reaction.

Loss of active materials is simply described using a following empirical equation [65]

$$\Delta\varepsilon_{s,n} = -k_{iso}\Delta\varepsilon_{SEI} \tag{3.49}$$

where k_{iso} is a dimensionless coefficient that describes how fast the active anode materials are isolated from chemical reactions due to electrical isolation of the SEI.

As the volume fraction of the active materials decreases, the electrode specific surface area a_k available for intercalation and side reactions decreases as charging continues. The reduction in the available active surface area is expressed empirically as [66],

$$a_n = a_n^0 \left[1 - \left(\frac{\varepsilon_n^0 - \varepsilon_n}{\varepsilon_n^0} \right)^{\zeta_n} \right] \tag{3.50}$$

where ζ_n is an empirical factor that represents the morphology of the side reaction product formed and it can be obtained through experiments.

Similarly, the solid phase diffusion coefficient can be expressed as,

$$D_{s,n} = D_{s,n}^0 \left[1 - \left(\frac{\varepsilon_n^0 - \varepsilon_n}{\varepsilon_n^0} \right)^{\zeta_n} (1 - \varepsilon_\delta) \right] \tag{3.51}$$

where $D_{s,n}^0$ is the initial solid phase diffusion coefficient and ε_δ is the porosity of the deposit.

Due to the irreversible parasitic side reactions, not all the cyclable lithium intercalates back to the electrodes. The lithium concentration in the electrode in next charge or discharge process is smaller in a given cycle than in the previous cycle. Assuming total number of intercalation sites remain constant, the volume of the electrode particles at any cycle can be related to the volume of the fresh particle as,

$$\frac{V_p C_{s,init}^N}{\varepsilon_{s,n}} = \frac{V_{p,0} C_{s,max}}{\varepsilon_{s,n,0}} \tag{3.52}$$

where ε_s is the volume fraction of the electrode and the volume of the electrode particle is calculated as,

$$\begin{aligned} V_{p,0} &= \frac{4\pi R_p^3}{3} \\ V_p &= \frac{4\pi(R_p + \delta_{film})^3}{3} \end{aligned} \tag{3.53}$$

From equations 3.52 and 3.53, the lithium concentration at any cycle can be expressed as,

$$C_{s,init}^N = C_{s,max}\left(\frac{R_p}{R_p + \delta_{film}}\right)^3 \frac{\varepsilon_{s,n}}{\varepsilon_{s,0}} \tag{3.54}$$

The electrode state of charge at the beginning of any charging cycle is

$$SOC_N = \frac{C_{s,init}^N}{C_{s,max}} \tag{3.55}$$

As the layer grows inside the porosity of the negative electrode, the available volume fraction of the electrolyte decreases. The electrolyte volume fraction in the negative electrode as a function of the film thickness is,

$$\varepsilon_{e,n}(t) = 1 - \varepsilon_{f,n} - \varepsilon_{s,n}\left[1 + \frac{3\delta_{film}(t)}{R_p}\right] \tag{3.56}$$

Change in the electrolyte volume fraction in the negative electrode will affect the effective electrolyte conductivity $(\kappa_{eff,n})$ and effective diffusivity $(D_{eff,n})$ of Li-ions in the negative electrode porosity,

$$\kappa_{eff,n} = \kappa_n \left[1 - \varepsilon_{f,n} - \varepsilon_{s,n} \left(1 + \frac{3\delta_{film}(t)}{R_p} \right) \right]^{brugg_n} \tag{3.57}$$

$$D_{eff,n} = D_n \left[1 - \varepsilon_{f,n} - \varepsilon_{s,n} \left(1 + \frac{3\delta_{film}(t)}{R_p} \right) \right]^{brugg_n} \tag{3.58}$$

From equations 3.57 and 3.58 with the aging of battery the effective conductivity and effective diffusivity tend to zero due to an increase of film thickness. Due to film formation over the electrode surface, Li-ion diffuses in and out of the electrode active material at a slower rate. The rate capability can be treated as a diffusion limited problem [49] and hence change in the diffusion coefficient over the cycling period can be used to compare the rate capability of porous and non-porous current collector based Li-ion battery.

3.5 Illustration of finite difference method (FDM)

Finite difference method is used to solve the partial differential equation involved because it is simpler and easier to implement. FDM converts differential equations into algebraic difference equations. For illustration purpose, equation 3.8 is solved using FDM.

Using forward difference method,

$$\frac{c_{s,k}^{avg}(i, j+1) - c_{s,k}^{avg}(i, j)}{\Delta t} = -3\frac{J_k(i, j)}{R_p} \tag{3.59}$$

Rearranging equation 3.59 the value of $c_{s,k}^{avg}(x,t)$ at a forward time can be expressed as,

$$c_{s,k}^{avg}(i,j+1) = c_{s,k}^{avg}(i,j) - 3\frac{J_k(i,j)}{R_p}\Delta t \tag{3.60}$$

Using equation 3.60 value at the forward time can be calculated. Δt and Δx are calculated as,

$$\Delta t = \frac{t}{m}$$
$$\Delta x = \frac{x}{n}$$

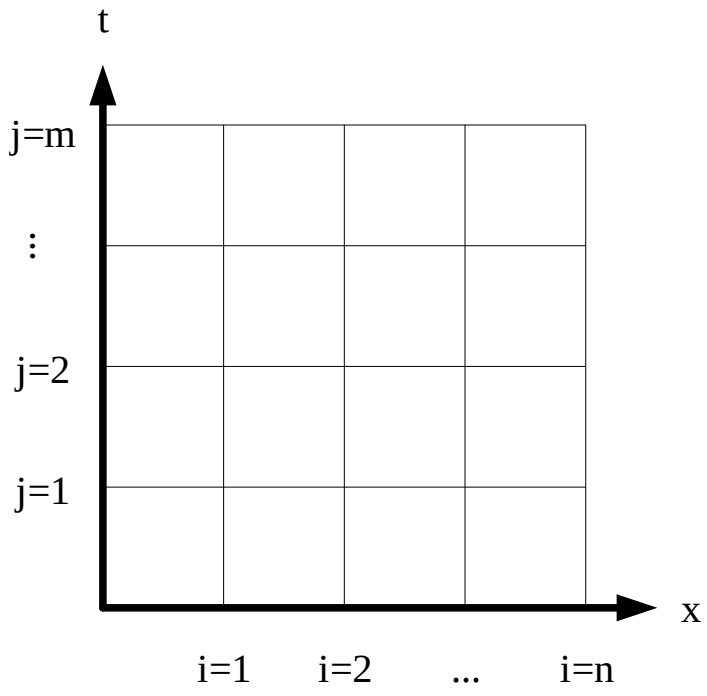

Figure 3.4. Grid lines used for discretization of partial differential equations.

Figure 3.4 shows the division of time axis and position axis into grid lines. The

value of time and position at any grid lines are calculated as,

$$t_j = (j-1)\Delta t, j = 1,2,...,m \tag{3.61}$$

$$x_i = (i-1)\Delta x, i = 1,2,...,n \tag{3.62}$$

For convergence of solutions, the choice of Δx and Δt should be such that $\Delta t/\Delta x^2 < 0.5$. In similar fashion, by using above explained process other differential equations can be converted into algebraic difference equations.

CHAPTER 4 RESULTS AND DISCUSSION

A half-cell battery model was developed in MATLAB. Figure 4.1 shows the half-cell model used for simulation studies. In this study, dimensions of coin cell casing were not considered. To simplify and avoid the complex computation, electrode averaged model developed by [56] was used with slight modifications. In [56] constant electrolyte concentration was assumed, but here average electrolyte concentration was considered. Finite difference method was used to solve the partial differential equations involved in the electrochemical model of the battery. Lithium titanate was considered as anode active material. The performance of porous current collector based half-cell was compared with foil type current collector based Li-ion half-cell. In the simulation, 3 V was taken as charge cut-off voltage and 1 V was taken as a discharge cut-off voltage. The comparison was done for discharge performance and capacity fading. The temperature effect on the battery performance was not considered. The porosity of the current collector was determined by image processing the experimentally obtained SEM image of porous copper foil.

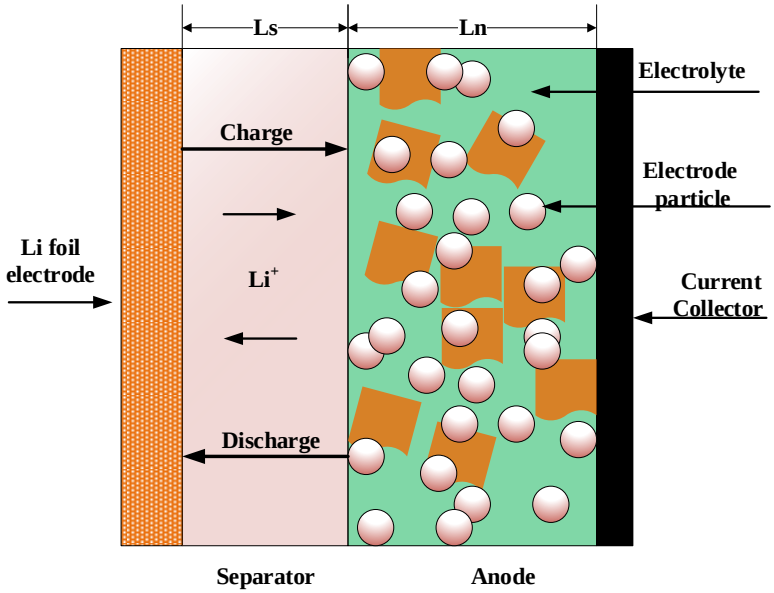

Figure 4.1. Half-cell model used for simulation.

4.1 Current collector porosity and distribution

Pores on the copper foil were created in the lab by the method of anodization [50] and characterized by SEM imaging. The watershed segmentation algorithm [67] was used to determine the porosity, average pore diameter and distribution of the pores by image processing in MATLAB. The image transformation applied on the grayscale image is a watershed in the study of image processing. The watershed transformation treats the image like a topographic map [68]. For calculating porosity, the original SEM image was converted to binary image format. Morphological analysis known as the *majority* was applied to retain the major structures. Finally, the watershed algorithm was applied to detect the pores formed on the copper foil.

Table 4.1 summarizes the value of the parameter obtained after applying the watershed algorithm. The calculated porosity is 0.598$\sim$ 0.6. Figure 4.2 shows the original SEM image, segmented image and pore's distribution. The distribution of pores from

experimental data looks random. Data obtained from image processing were tested against uniform distribution and normal distribution using Kolmogorov-Smirnov test [69]. The p-values obtained at 95% level of significance for uniform distribution test and normal distribution test were 1.2053×10^{-4} and 0.0226. The results were against the null hypothesis for both the test. It means the data show random distribution. However, for simplicity, the current collector pores distribution was assumed uniform.

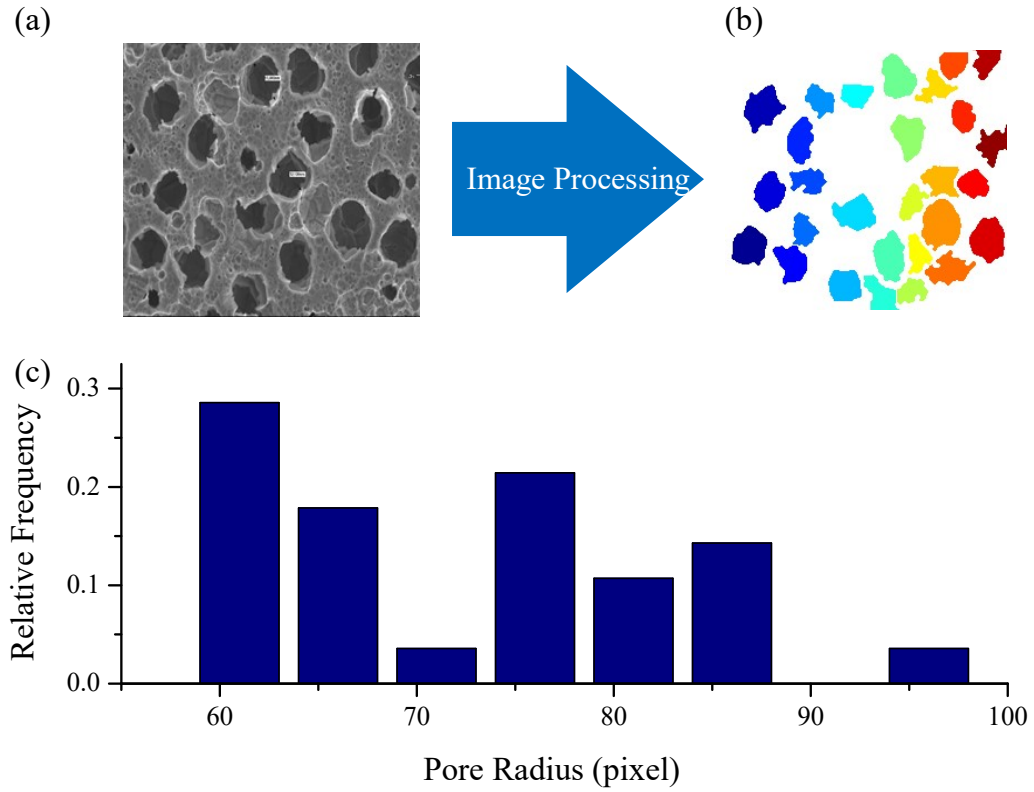

Figure 4.2. (a) Original SEM image, (b) segmented image and (c) pore distribution.

Table 4.1. Summary of results obtained from image processing.

Parameter	value
Porosity	0.598
Average Pore Radius(pixel)	72.93
Standard Deviation	10.58

4.2 Model validation

Change in volume fraction of active material is one of the notable changes with the use of porous current collector. For the model validation, the volume fraction of electrode active material was calculated using the proposed model. The result was compared with the electrode active material computed using an earlier model reported [70]. Model in [70] calculates the volume fraction of electrode's active materials using the relation,

$$\varepsilon_k = \frac{4}{3}\frac{\pi(R_p)^3 K_k}{A_k L_k} \tag{4.1}$$

where K_k is the number of spherical particles in k^{th} electrode calculated as,

$$K_k = \frac{3}{4}\frac{M_k}{\pi R_p^3 \rho_k} \tag{4.2}$$

In table 4.2, both the models give the same volume fraction of anode active material with the porous and non-porous current collectors. This validates the proposed equations that were adjusted for the volume fraction of active materials. Here only the volume fraction of anode active material was compared because copper as anode current collector was made porous.

Table 4.2. Anode active material volume fraction for the porous and non-porous current collectors based Li-ion battery.

	Proposed Model	Model in [70]
Porous Current Collector	0.77184	0.77184
Non-porous Current Collector	0.4824	0.4824

For validating the increase in effective conductivity of electrode using porous

current collector, a half-cell was prepared using lithium titanate as anode material. Electrochemical impedance spectroscopy (EIS) measurements were performed. Transport resistances of Li-ion batteries with porous and non-porous current collectors were compared. Figure 4.3 shows the EIS plots of lithium titanate based Li-ion half-cells. The transport resistance is $\sim 200\ \Omega$ for non-porous current collector based cells and $\sim 150\ \Omega$ for porous current collector based cells. Several researchers working on the modified current collector have obtained the similar result [33]. They ascribed the higher electrode specific area to be the reason for smaller transfer resistance in porous current collector cells. The model proposed here predicts higher electrode specific area for porous current collector cells as expressed in equations 3.3 and 3.4. The use of porous current collector increases the transport conductivity of the anode electrode. The increase in effective electrode conductivity was also predicted by the proposed model.

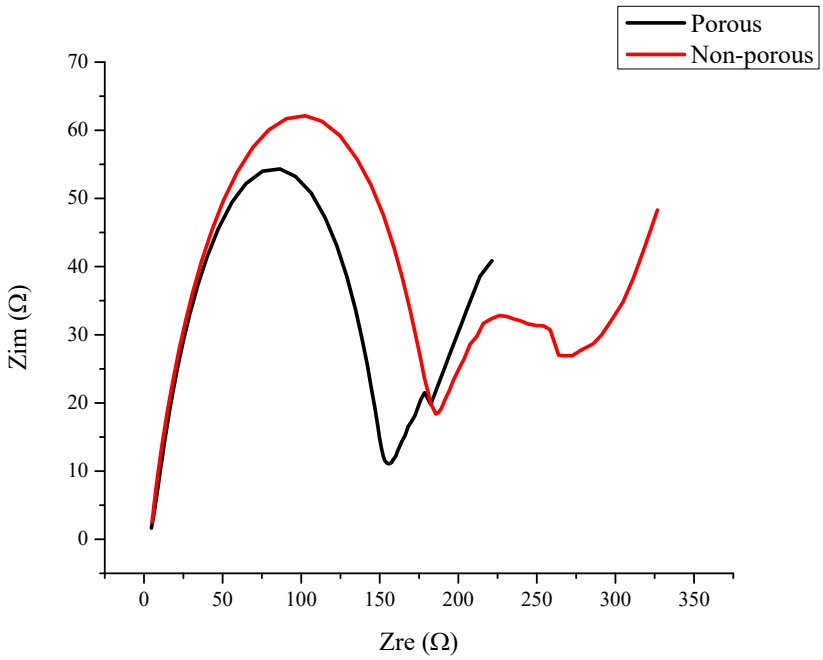

Figure 4.3. EIS plots for lithium titanate based half-cells for porous and non-porous current collector.

4.3 Discharge performance

Discharge performance comparison was done using the adjusted equations in the electrode averaged model (EAM). The explanation of EAM is given in chapter 3 section 3.3. The electrode equilibrium potential $U_{ref,n}$ was determined to fit the experimental data. As seen in figure 4.4, the discharge curve can be divided into three portions with two turning points. The first portion is the region before first turning point. The shape of this portion is mainly determined by the internal resistance of the battery. The second portion is regarded as the voltage of the discharge curve. It is the stable discharge period of a battery. The third portion after second turning point indicates the battery is reaching the end of discharge.

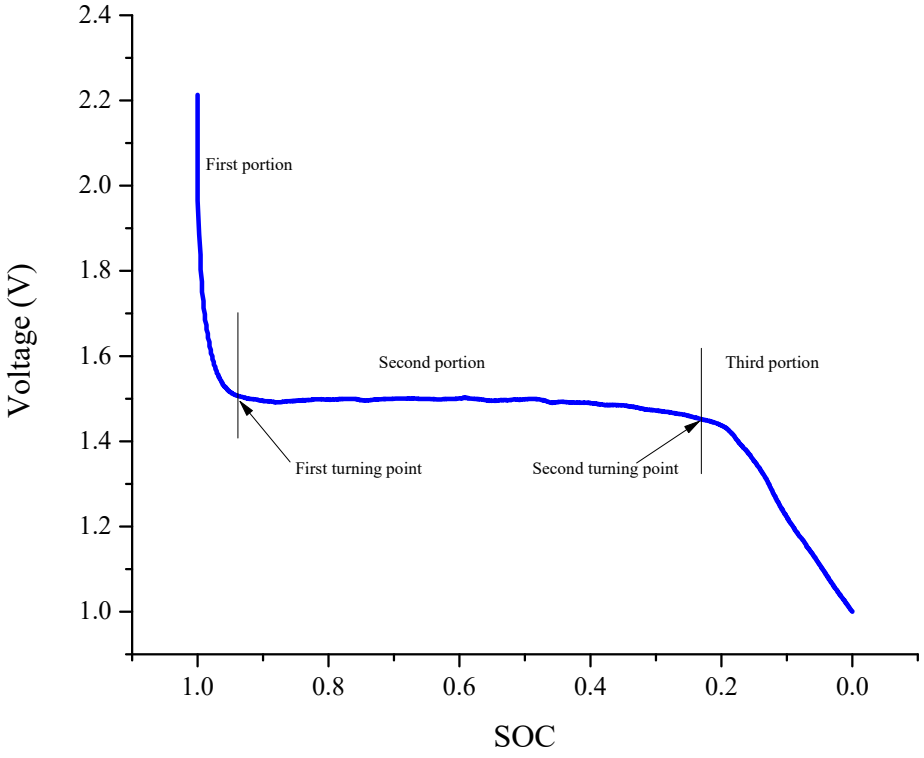

Figure 4.4. A discharge curve of a battery obtained plotting experimental data.

The electrode equilibrium potential was determined separately fitting these three portions of discharge curve using the method explained in the literature [71]. The fitted expression for $U_{ref,n}$ as a function of SOC is

$$\begin{aligned} U_{ref,n} = {} & 1.073 - 0.5685\exp(-72.1839SOC) - 3.40782\exp(-25546.8235SOC) \\ & + 8.427\times10^{-12}\exp(25.88SOC) \end{aligned} \tag{4.3}$$

For discharge performance, the variation of energy with cell voltage was studied. The energy density of the cell was calculated by the trapezoidal approximation:

$$E_{cell} = \frac{1}{M_{cell}V_n}\int_0^{t_d} V_{cell}(t)Idt \approx I\sum_{k=0}^{n}\frac{V_{k+1}+V_k}{2}(t_{k+1}-t_k) \tag{4.4}$$

where I ($I = Q_n M_n$) denotes the cell current, k is the time step number, t_d is a time of discharge and n is the number of time steps needed to reach the cutoff voltage and V_n is nominal voltage. The cell mass, in turn, was calculated as:

$$\begin{aligned} M_{cell} &= M_p + M_{sep} + M_n + M_{cc} \\ M_p &= \rho_p L_p(1-\varepsilon_p-\varepsilon_{fp}) \\ M_{sep} &= \rho_s(L_p\varepsilon_p + L_{sep} + L_n\varepsilon_n) + \rho_f(L_p\varepsilon_{fp} + L_n\varepsilon_{fn}) \\ M_n &= \rho_n L_n(1-\varepsilon_n-\varepsilon_{fn}) + \rho_n\varepsilon_{cc}(1-\varepsilon_n-\varepsilon_{fn})L_{cc} \\ M_{cc} &= \rho_{cc_n}L_{cc}(1-\varepsilon_{cc}) + \rho_{cc_p}L_{cc} \end{aligned} \tag{4.5}$$

In equation 4.5, M_p, M_{sep}, M_n and M_{cc} are the mass of the positive active materials,

negative active materials, electrolyte and current collectors respectively. The mass of each component is a function of its thickness and porosity that make up its composition. The mass equations were adjusted for the porous current collector case at the anode side.

Figure 4.5 (a) and (b) show the simulation results and experimental results for specific capacity and voltage and Figure 4.5 (c) and (d) show the simulation results for dimensionless surface charge concentration and state of charge at the 0.1 C discharge rate. The voltage plateau and the final discharge capacity predicted by the model agree with experimental data. The specific capacity of porous current collector obtained is higher than 175 mAh/g that is the theoretical capacity for lithium titanate based Li-ion battery. This is because porous current collector reaches the end of discharge at a slower rate due to the slower reduction of surface charge concentration. The slower rate of discharge for the porous current collector is due to the improved transport properties and electrode specific surface area. In addition, the porous current collector reduces the insignificant mass that is the mass of copper.

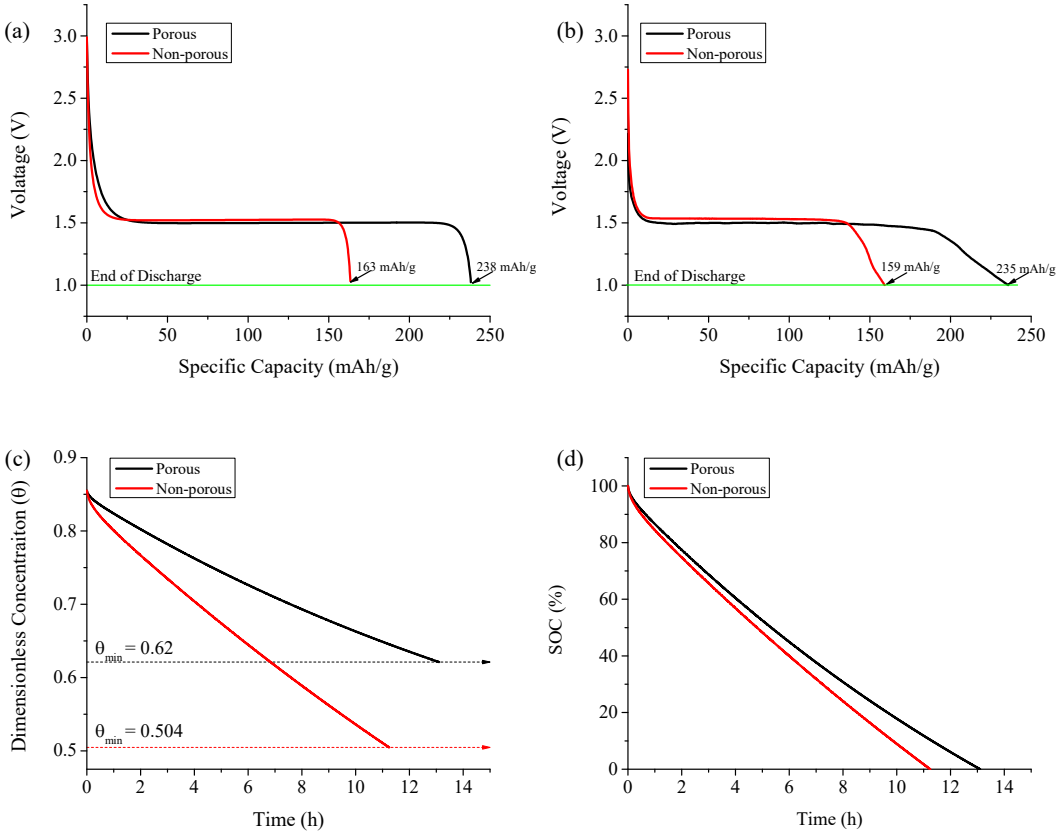

Figure 4.5. (a) Simulation discharge performance, (b) experimental discharge performance, (c) dimensionless surface charge concentration and (d) state of charge results for the 0.1 C discharge rate.

4.3.1 Discharging at different C-rates

The battery was discharged at different C-rates and the obtained discharge capacities were compared with experimental capacities taken from [50]. Figure 4.6 shows the radar plot to compare the discharge capacities at different C-rates for a porous current collector based Li-ion battery. The accuracy of the model is decreasing for increasing C-rates. Table 4.4 shows the relative error in capacity obtained from the simulation at different C-rates. The reason for increasing error at higher currents is terminal voltage reaches the cutoff voltage earlier than the calculated time for the given C-rates.

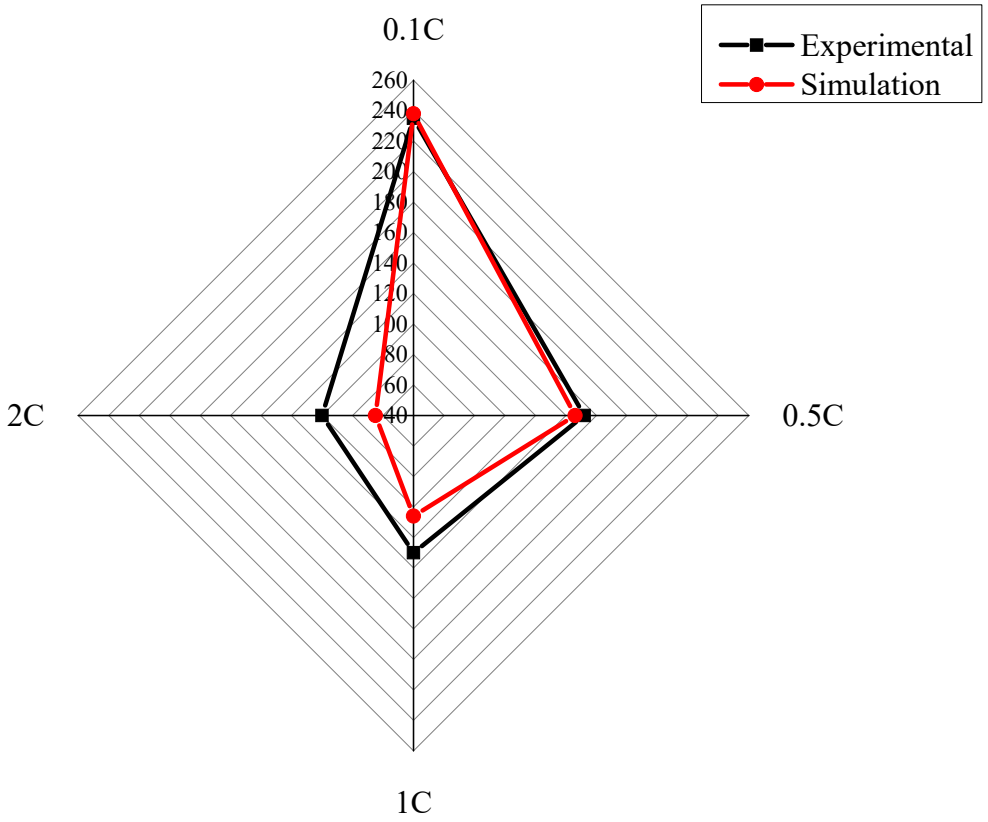

Figure 4.6. Radar plot to compare the accuracy of the model with respect to experimental data at different C-rates.

Table 4.3. Error analysis at different C-rates of discharge.

Rate	Experimental [50]	Simulation	Error
0.1C	235	238	1.27%
0.5C	152	146	3.95%
1C	130	106	18.67%
2C	100	65	35%

4.3.2 Effect of cycling on capacity

To study the effect of cycling on the capacity of the battery, the simulation was performed at the 1C rate for 150 cycles. Figure 4.7 shows the discharge performance of non-porous current collector based Li-ion battery at 1^{st} and 150^{th} cycles. In the figure, with the increasing cycle number, there is a decrease in discharge capacity and initial

discharge voltage. The reason for the drop of initial voltage is the increase of the high frequency resistance that is dc resistance [72]. The loss in capacity is known as capacity fading. The reasons for capacity fade in Li-ion batteries are explored in next sections.

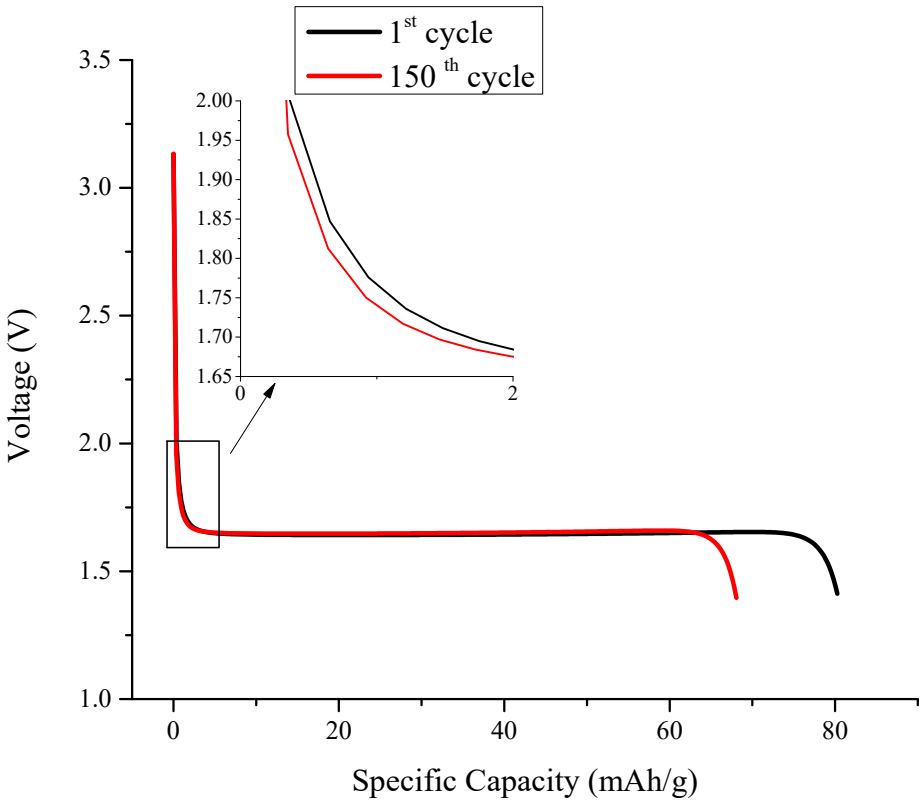

Figure 4.7. Effect of cycling on discharge performance.

4.4 Capacity fade

The irreversible loss in capacity of the battery occurs due to storage and cycling. This loss in capacity is called capacity fade. Side reactions taking place inside the battery are the cause for the degradation of battery performance. Solid electrolyte interphase layer growth and the lithium plating are the two major side reactions occurring inside the battery. In this work, capacity fade due to lithium plating was not considered. Capacity

fading simulation was performed using the model explained in the literature [64] with slight modifications. In literature [64], they vary the state of charge (SOC) of the battery between 0% and 100% in the steps of 2% and computes the lithiation state θ_n of anode according to

$$\theta_n = \theta_{n,min} + soc\left(\theta_{n,max} - \theta_{n,min}\right) \tag{4.6}$$

where θ_{max} and θ_{min} are the stoichiometric limits of anode lithiation. However, in this work, the surface charge concentration was computed using the Wang and Srinivasan [73] empirical formula to account for the diffusion inside solid spherical particles. The empirical relation is

$$C^{*}_{s,k}(t) = C^{avg}_{s,k}(t) + J^{Li}\frac{-R_P}{5a_nFD_s}\left[1 - \exp\left(-\frac{20}{3}\frac{\sqrt{D_s t}}{R_P}\right)\right] \tag{4.7}$$

The average concentration $C^{avg}_{s,k}(t)$ was calculated using the equation 3.8 and the state of charge of the battery was computed according to

$$SOC = \frac{\theta - \theta_{min}}{\theta_{max} - \theta_{min}} \tag{4.8}$$

Total capacity fade can be divide into the rate capability loss, the capacity loss due to loss of active materials and loss due to increase in the polarization and charge transfer resistance with cycling. State of charge of the limiting electrode accounts for loss due to active materials loss, solid phase diffusion coefficient account for capacity loss due to rate capability and film resistance account for the increase of polarization and charge transfer resistance with cycling [49]. In this work, variations of state of charge and solid phase

diffusion coefficient of the anode and the rate of growth of film resistance with cycling are compared.

4.4.1 Capacity fade model validation

The growth of the film follows parabolic growth law [74], which means that the rate of increase in the thickness of the passivating layer is inversely proportional to the thickness of the layer. To validate the model, the film thickness data obtained are fitted to test if the data show parabolic growth rate.

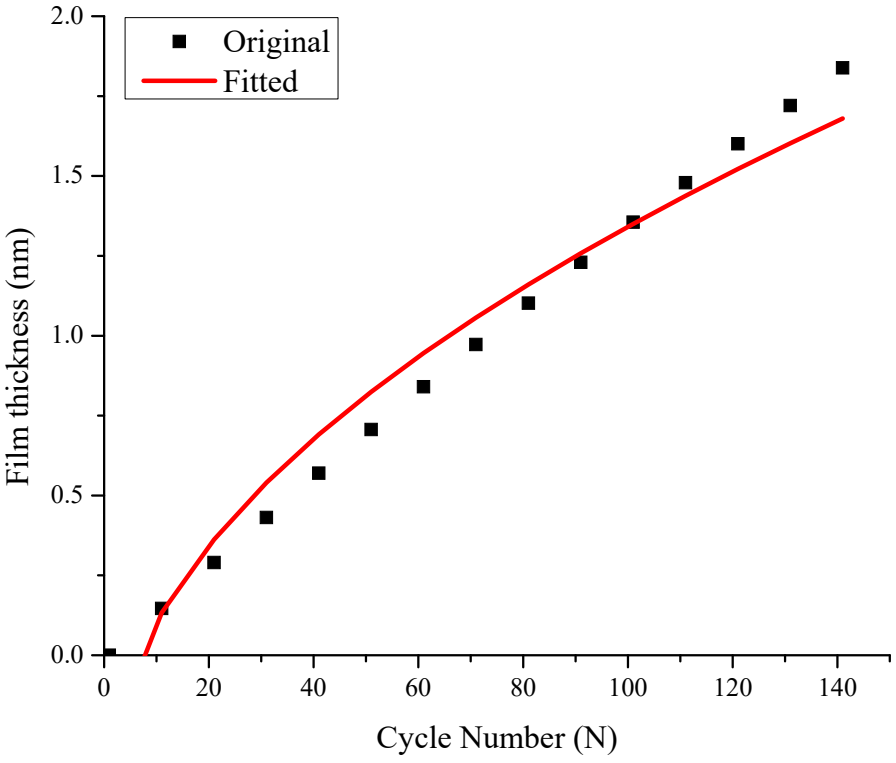

Figure 4.8. Curve fitting of simulation data.

Figure 4.8 shows the original data and the fitted data. The fitted data model is

$$\hat{\delta}_{film} = 0.1807\sqrt{N} - 0.4659 \tag{4.9}$$

and the goodness of fit parameters are,

Table 4.4. Goodness of fit.

Sum of square error (SSE):	0.1966
R-square:	0.9592
Adjusted R-square:	0.9561
Root mean square error (RMSE):	0.123

Equation 4.9 and goodness of fit parameters suggest the growth of film predicted by simulation model follows the parabolic growth rate. Many researchers studying the failure of Li-ion battery have identified the square root fitting of film thickness against cycle number and have demonstrated this model fit experimental data very well [41], [49], [75], [76].

4.4.2 Comparison of film growth

In this work, lithium plating is not considered. So, the surface film contains SEI only. Figure 4.9 compares the SEI thickness and film resistance growth with cycling. The increase of the SEI thickness and resistance over each charging cycle is higher for the non-porous current collector than for porous current collector based Li-ion cells. This is because the porous current collector has higher specific electrode surface area and better transport properties due to which the intercalation and side reactions occur at a slower rate in porous current collector cells. The slower rate of side reactions leads to the slow formation of SEI layer on the surface of electrode particles of porous current collector cells.

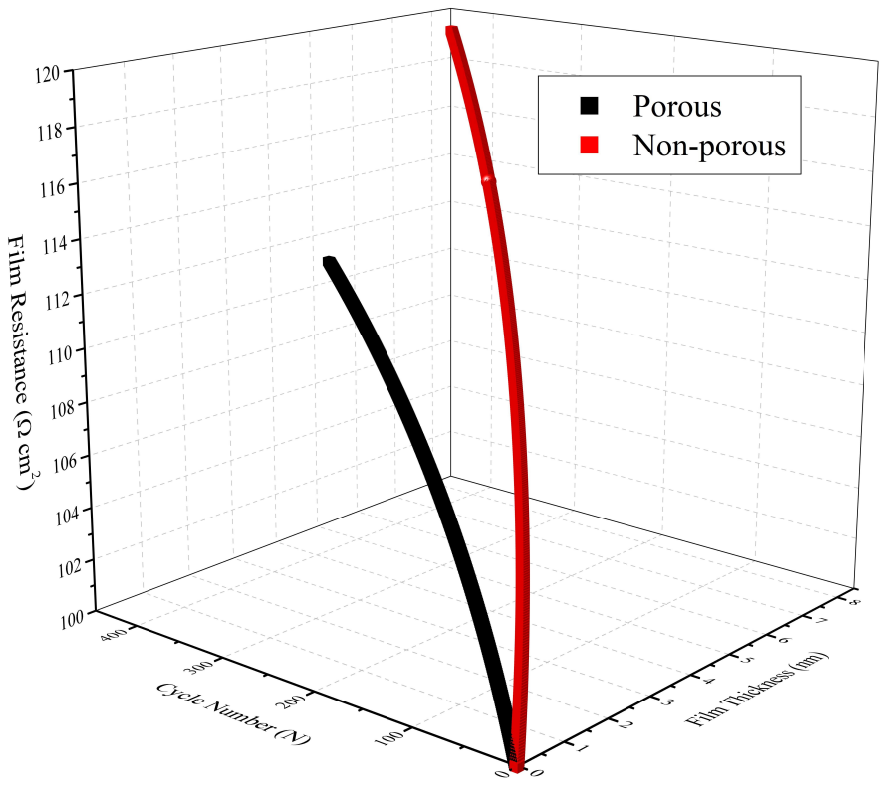

Figure 4.9. Variation of the film resistance and SEI thickness with cycling.

According to the literature [49], film resistance account for the capacity fade due to an increase of polarization and charge transfer resistance. Hence, the capacity fading due to an increase of polarization and charge transfer resistance is less for porous current collector cells.

4.4.3 Comparison of electrode state of charge and solid phase diffusion coefficient

The variations of electrode state of charge and solid phase diffusion coefficient due to cycling were calculated using the equations 3.55 and 3.51. The empirical parameter ζ_n that represents the morphology of side reaction product was assumed to be 1 and porosity of deposit ε_δ was assumed to be 0. Initial diffusion coefficient was taken to be $2 \times 10^{-16} \mathrm{m^2 s^{-1}}$ for both type of cells. Figure 4.10 compares the variation of electrode

state of charge and diffusion coefficient. The decay of electrode state of charge and diffusion coefficient is faster for non-porous current collector cells. The decay of electrode initial state of charge depends on the loss of surface concentration from solid particles which in turns depends upon the growth of the film. As seen in the previous section, the film thickens faster in the case of non-porous current collector cells. The decay of diffusion coefficient depends on the relative change in the volume fractions of solid particles. As seen in equation 3.49, the reduction in volume fraction of solid particles depends upon the volume fraction of SEI formed, which in turn depends upon the rate of side reactions. Side reactions occur at a faster rate in non-porous current collector cells due to smaller specific electrode area compared to porous current collector cells.

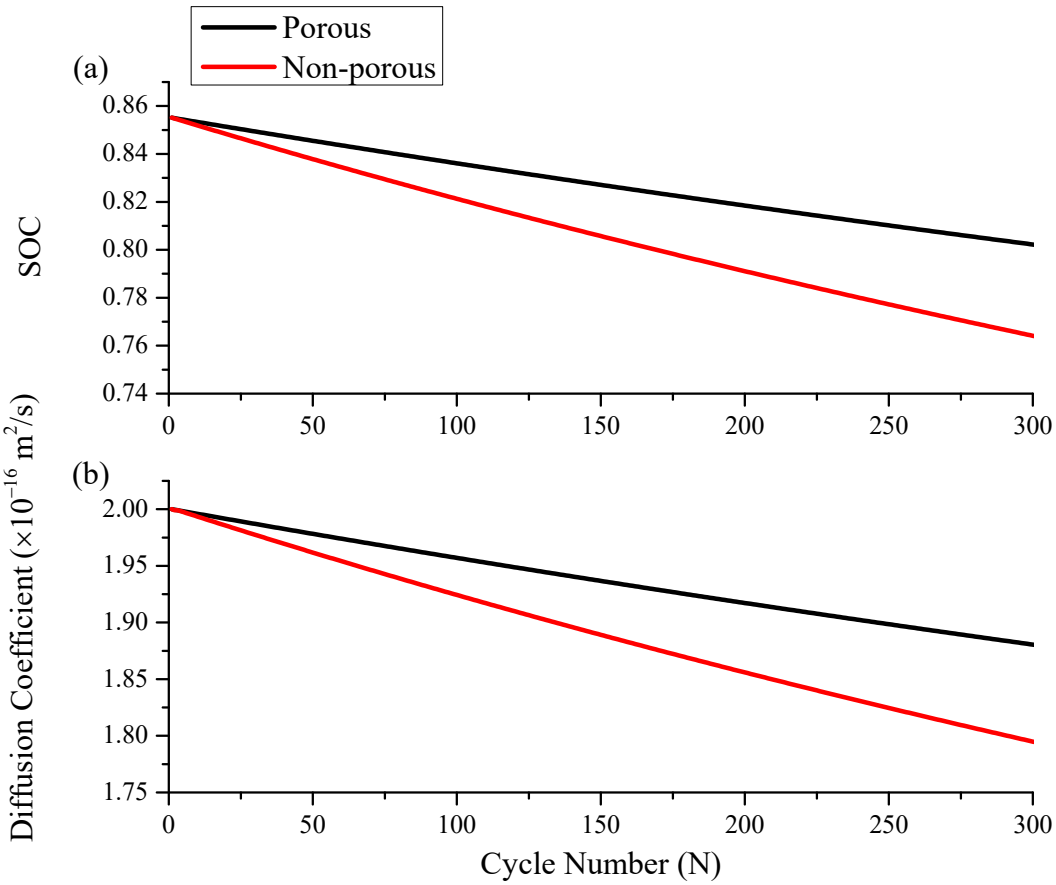

Figure 4.10. (a) Electrode state of charge and (b) diffusion coefficient.

According to the literature [49], electrode state of charge and solid phase diffusion coefficient account for the capacity fade due to loss of active materials and loss of rate capability. Hence, the capacity fade due to loss of active materials and loss of rate capability is higher in non-porous current collector cells.

4.5 State of health (SOH)

SOH indicates how much of the useful lifetime of the battery has been consumed and how much remains before it must be replaced. Any parameter that changes significantly with age such as cell impedance can be used to calculate the SOH of the battery [77]. In this work, SOH was calculated by comparing the cycled capacity of the battery with an initial capacity. SOH was calculated as

$$SOH = \frac{Q_i}{Q_{max}} \tag{4.10}$$

Q_i is the capacity at the i^{th} discharge cycle and Q_{max} is the discharge capacity of the fresh cell. The capacity obtained from the simulation for discharge performance was taken as Q_{max} and Q_i was calculated according to

$$Q_i = Q_{max} - Q_{loss} \tag{4.11}$$

where the loss in capacity Q_{loss} was calculated as,

$$Q_{loss} = C_{s,max} - C^N_{s,init} \tag{4.12}$$

$C^N_{s,init}$ was calculated using the equation 3.54. Equation 4.12 gives the value in $molm^{-3}$. The value of loss can be expressed in AH as

$$Q_{loss}(AH) = \frac{Q_{loss}(molm^{-3})AL_n}{F\varepsilon_{sn}} \tag{4.13}$$

For SOH calculation, the battery was completely discharged at the 0.1 C rate. The limit of SOH to predict the end of useful life was set as 80% of initial capacity [78]. Figure 4.11 shows the variation of SOH with cycling for each type of cell. The non-porous based Li-ion cell reaches the end of useful life quicker than the porous based Li-ion cells. The porous current collector cells take approximately 100 more cycles to reach the end of useful life than the non-porous current collector cells. The reason is that the SEI growth rate is slower in the porous current collector based cells due to which loss of irreversible lithium surface charge concentration is less in the porous current collector cells. Lesser irreversible lithium surface charge concentration loss leads to a lesser irreversible capacity loss in porous current collector cells. Previous work [79] has shown a reduced irreversible capacity loss by using foam-type three-dimensional current collector experimentally.

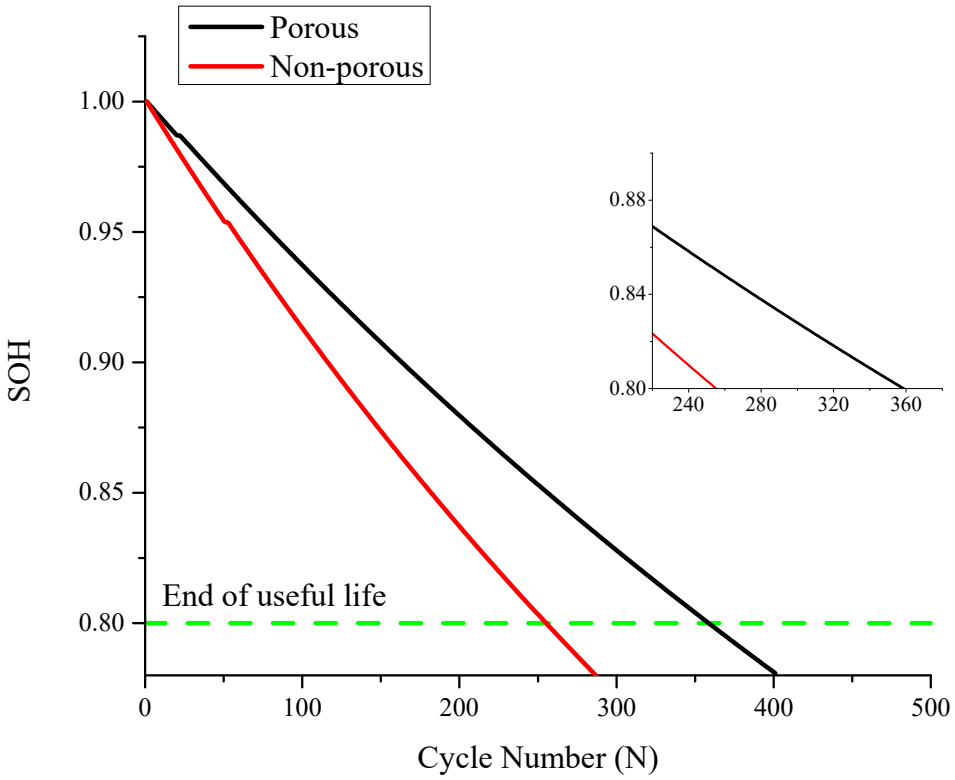

Figure 4.11. SOH vs cycle number of non-porous and porous current collector.

From above analysis, it can be concluded that the use of the porous current collector improves the discharge performance and capacity fading in Li-ion batteries.

Table 4.5. Battery parameters used in the simulation study.

	Unit	Negative Electrode	Separator
Geometry and volume fractions: [80]			
Electrode thickness(L_k)	μm	100	25
Current Collector thickness (L_{cc})	μm	10	
Particle radius ($R_{s,k}$)	μm	2	
Porosity (ε_k)		0.485	0.724
Current collector porosity (ε_{cc})		0.6	
Volume fraction of fillers ($\varepsilon_{f,k}$)		0.0326	
Kinetic trasport properties:			
Charge transfer coefficients (α_k)		0.5	
Electronic conductivity (σ_k) [81]	Sm^{-1}	100	
Ionic conductivity(κ_S)	Sm^{-1}	Equation3.18	Equation3.18
Solid phase diffusion coefficient (D_S)	m^2s^{-1}	2×10^{-16}	
Electrolyte phase diffusion coefficient (D_e) [81]	m^2s^{-1}	7.5×10^{-10}	7.5×10^{-10}
Transference number (t_+) [81]		0.363	
Bruggeman's coefficient(brugg)		1.5	1.5
Li^+ concentrations: [80]			
Maximum solid phase concentration ($C_{s,max}$)	$molm^{-3}$	30555	
Initial solid phase concentration ($C_{s,init}$)	$molm^{-3}$	26128	
Initial concentration in electrolyte(C_e^{int})	$molm^{-3}$	1000	1000
Side reaction parameters:			
Initial SEI resistance (Ω_{SEI}) [19]	Ωcm^2	100	
Exchange current density(i_{os}) [19]	Am^2	1.5×10^{-8}	
Molecular Weight of SEI layer (M_{SEI})[82]	$kgmol^{-1}$	7.3×10^4	
Density of SEI layer (ρ_{SEI}) [82]	kgm^{-3}	2.1×10^3	
Conductivity of SEI(κ_{SEI})	Sm^{-1}	3.79×10^{-6}	
Side reaction reference voltage ($U_{ref,side}$)	V	0.2	
Isolation rate of active anode material due to SEI (k_{iso}) [65]		27.3	
Other parameters:			
Faraday's constant (F)	$Cmol^{-1}$		96487
Density of active materials (ρ_n)	kgm^{-3}	3430	
Density of electrolyte (ρ_s) [18]	kgm^{-3}		1100
Density of Copper	kgm^{-3}	8940	
Theoretical Specific Capacity(Q_n)	$mAhg^{-1}$	175	
Temperature (T)	K	300	300
Universal gas constant (R)	$Jmol^{-1}K^{-1}$	8.314	8.314

CHAPTER 5 CONCLUSIONS

5.1 Summary

The energy consumption has increased due to population growth and improvement in a living standard. As of now, fossil fuels are the main source of energy. However, fossil fuels are not environmentally friendly as they emit carbon dioxide, which is major greenhouse gas when burnt. Fossil fuels are forecasted to deplete completely if the current trend of use persists. Researchers are focusing on renewable energy as they don't pose environmental threats. However, renewable energy is intermittent in nature. A suitable medium is required to store the energy produced from renewable energy sources. Batteries, supercapacitors, flywheels, fuel cells are some of the storage devices. The battery is the focus of this thesis.

Batteries are mainly classified as rechargeable and non-rechargeable batteries. Among different rechargeable batteries chemistry, Li-ion batteries are most popular because of their higher energy density and long life. The demand for high capacity and the durable Li-ion battery is increasing in electronic gadgets, electric vehicles and renewable energy storage system. The future Li-ion battery should be smaller in size with higher energy and power density.

Existing literature suggests the energy density of Li-ion battery can be increased either by finding the new electrode materials or modifying the design of the battery. Design modification is considered in this thesis. Increasing the electrode thickness is the straightforward method to increase the energy density of the Li-ion battery. However, increased thickness impairs the electrolyte-phase mass transfer which makes Li-ion

battery unsuitable for different applications [19], [24], [25]. Different researchers tried varying electrode porosity model to increase the energy density of the battery; however, they observed very little improvement in the energy density compared to constant electrode porosity [32]. Recently, researchers [33], [34] are focusing on the modifications of the current collector. They observed that use of porous current collector increases the energy density and capacity retention of Li-ion battery.

In this thesis, existing battery model equations were adjusted for the case of porous current collector based batteries. A simulation study was performed to compare the capacity fading of porous current collector based Li-ion battery with foil type current collector based battery. Half-cell model was developed in MATLAB. The porosity of the current collector was determined by applying the watershed algorithm on the experimentally obtained SEM image of porous copper.

5.2 Conclusion

The P2D battery model equations were adjusted for the case of porous current collector based Li-ion battery. Adjusted equations were used in electrode averaged model (EAM) to compare the discharge performance. The image processing of SEM characterization image of porous copper showed the random distribution of pores on the current collector; however, for simplicity and to avoid computational burden uniform distribution was assumed. Simulation and EIS measurement showed higher transport properties of porous current collector based Li-ion battery. Simulation results showed the rate of the SEI thickness growth was slower in porous current collector than in the non-porous current collector battery. Capacity fade due to an increase of polarization and

transfer resistance, due to loss of active materials and loss of rate capability was less in porous current collector cells. Further, porous current collector cell took approximately 100 more cycles to reach the end of useful life compared to non-porous current collector cell. Thus, with the use of porous current collector energy density and life cycle of the battery can be increased without the need for significant modifications in battery structure.

5.3 Future Work

In this work, pores on the current collector were assumed to be uniform, depth of the pores on the current collector was not considered. Capacity fading was assumed to be caused solely due to the SEI growth during the charging cycle, the effect of the gas evolution and lithium plating were neglected. The accuracy of the model at high C-rates was poor, that can be improved by using advanced battery model for simulation. In future, the actual distribution of pores of current collector and depth of the pores can be considered and the effect of the gas evolution and the lithium plating can be modeled for more accurate comparison of the capacity fading. A thermal model was not considered here, the temperature rise can be compared. At present time battery explosion due to temperature rise is a serious problem, if the use of the porous current collector improves the thermal performance of battery it can be one of the solutions to reduce the battery explosion due to temperature rise.

REFERENCES

[1] *Eia projects 482040*, Accessed: April 26, 2017. [Online]. Available: https://www.eia.gov/todayinenergy/detail.php?id=26212.

[2] Wikipedia, *Fossil fuel— Wikipedia, The Free Encyclopedia*, Accessed: April 26, 2017. [Online]. Available: https://en.wikipedia.org/wiki/Fossil_fuel.

[3] D. saheb Koussa and M. Koussa, "Ghgs (greenhouse gases) emission and economic analysis of a gcres (grid-connected renewable energy system) in the arid region, algeria," *Energy*, vol. 102, pp. 216–230, 2016.

[4] *Man-made co2 emissions*, Accessed: April 26, 2017. [Online]. Available: www.oica.net/category/climate-change-and-co2/.

[5] A. Gurung, K. Chen, R. Khan, S. S. Abdulkarim, G. Varnekar, R. Pathak, R. Naderi, and Q. Qiao, "Highly efficient perovskite solar cell photocharging of lithium ion battery using dc–dc booster," *Advanced Energy Materials*, 2017.

[6] D. Linden, "Handbook of batteries and fuel cells," *New York, McGraw-Hill Book Co., 1984, 1075 p. No individual items are abstracted in this volume.*, vol. 1, 1984.

[7] P. Van den Bossche, F. Vergels, J. Van Mierlo, J. Matheys, and W. Van Autenboer, "Subat: An assessment of sustainable battery technology," *Journal of power sources*, vol. 162, no. 2, pp. 913–919, 2006.

[8] B. J. Landi, M. J. Ganter, C. D. Cress, R. A. DiLeo, and R. P. Raffaelle, "Carbon nanotubes for lithium ion batteries," *Energy & Environmental Science*, vol. 2, no. 6, pp. 638–654, 2009.

[9] C Scuilla, "The commercialization of lithium battery technology," *Proceedings of Battcon*, 2007.

[10] A. Yoshino, "The birth of the lithium-ion battery," *Angewandte Chemie International Edition*, vol. 51, no. 24, pp. 5798–5800, 2012.

[11] D. Deng, "Li-ion batteries: Basics, progress, and challenges," *Energy Science & Engineering*, vol. 3, no. 5, pp. 385–418, 2015.

[12] R. Naderi, A. Gurung, Z. Zhou, G. Varnekar, K. Chen, J. Zai, X. Qian, and Q. Qiao, "Activation of passive nanofillers in composite polymer electrolyte for higher performance lithium-ion batteries," *Advanced Sustainable Systems*, 2017.

[13] A. Gurung, R. Naderi, B. Vaagensmith, G. Varnekar, Z. Zhou, H. Elbohy, and Q. Qiao, "Tin selenide–multi-walled carbon nanotubes hybrid anodes for high performance lithium-ion batteries," *Electrochimica Acta*, vol. 211, pp. 720–725, 2016.

[14] Z. Zhou, H. Zhang, Y. Zhou, H. Qiao, A. Gurung, R. Naderi, H. Elbohy, A. L. Smirnova, H. Lu, S. Chen, *et al.*, "Binder free hierarchical mesoporous carbon foam for high performance lithium ion battery," *Scientific Reports*, vol. 7, 2017.

[15] J.-M. Tarascon and M. Armand, "Issues and challenges facing rechargeable lithium batteries," *Nature*, vol. 414, no. 6861, pp. 359–367, 2001.

[16] B. Y. Liaw, G. Nagasubramanian, R. G. Jungst, and D. H. Doughty, "Modeling of lithium ion cells—a simple equivalent-circuit model approach," *Solid state ionics*, vol. 175, no. 1, pp. 835–839, 2004.

[17] G. L. Plett, "Extended kalman filtering for battery management systems of lipb-based hev battery packs: Part 3. state and parameter estimation," *Journal of Power sources*, vol. 134, no. 2, pp. 277–292, 2004.

[18] M. Torchio, L. Magni, R. B. Gopaluni, R. D. Braatz, and D. M. Raimondo, "Lionsimba: A matlab framework based on a finite volume model suitable for li-ion battery design, simulation, and control," *Journal of The Electrochemical Society*, vol. 163, no. 7, A1192–A1205, 2016.

[19] M. Doyle, T. F. Fuller, and J. Newman, "Modeling of galvanostatic charge and discharge of the lithium/polymer/insertion cell," *Journal of the Electrochemical Society*, vol. 140, no. 6, pp. 1526–1533, 1993.

[20] N. Xue, W. Du, A. Gupta, W. Shyy, A. M. Sastry, and J. R. Martins, "Optimization of a single lithium-ion battery cell with a gradient-based algorithm," *Journal of The Electrochemical Society*, vol. 160, no. 8, A1071–A1078, 2013.

[21] V. D. Bruggeman, "Berechnung verschiedener physikalischer konstanten von heterogenen substanzen. i. dielektrizitätskonstanten und leitfähigkeiten der mischkörper aus isotropen substanzen," *Annalen der physik*, vol. 416, no. 7, pp. 636–664, 1935.

[22] V. R. Subramanian, V. Boovaragavan, and V. D. Diwakar, "Toward real-time simulation of physics based lithium-ion battery models," *Electrochemical and Solid-State Letters*, vol. 10, no. 11, A255–A260, 2007.

[23] A. Seaman, T.-S. Dao, and J. McPhee, "A survey of mathematics-based equivalent-circuit and electrochemical battery models for hybrid and electric vehicle simulation," *Journal of Power Sources*, vol. 256, pp. 410–423, 2014.

[24] W. Tiedemann and J. Newman, "Maximum effective capacity in an ohmically limited porous electrode," *Journal of The Electrochemical Society*, vol. 122, no. 11, pp. 1482–1485, 1975.

[25] V. Srinivasan and J. Newman, "Design and optimization of a natural graphite/iron phosphate lithium-ion cell," *Journal of the Electrochemical Society*, vol. 151, no. 10, A1530–A1538, 2004.

[26] M. Doyle, J. Newman, A. S. Gozdz, C. N. Schmutz, and J.-M. Tarascon, "Comparison of modeling predictions with experimental data from plastic lithium ion cells," *Journal of the Electrochemical Society*, vol. 143, no. 6, pp. 1890–1903, 1996.

[27] V. Srinivasan and J. Newman, "Discharge model for the lithium iron-phosphate electrode," *Journal of the Electrochemical Society*, vol. 151, no. 10, A1517–A1529, 2004.

[28] L. O. Valøen and J. N. Reimers, "Transport properties of lipf6-based li-ion battery electrolytes," *Journal of The Electrochemical Society*, vol. 152, no. 5, A882–A891, 2005.

[29] S. Stewart, P. Albertus, V. Srinivasan, I. Plitz, N. Pereira, G. Amatucci, and J. Newman, "Optimizing the performance of lithium titanate spinel paired with activated carbon or iron phosphate," *Journal of The Electrochemical Society*, vol. 155, no. 3, A253–A261, 2008.

[30] V. Ramadesigan, R. N. Methekar, F. Latinwo, R. D. Braatz, and V. R. Subramanian, "Optimal porosity distribution for minimized ohmic drop across a porous electrode," *Journal of The Electrochemical Society*, vol. 157, no. 12, A1328–A1334, 2010.

[31] S. Golmon, K. Maute, and M. L. Dunn, "A design optimization methodology for li+ batteries," *Journal of Power Sources*, vol. 253, pp. 239–250, 2014.

[32] Y. Dai and V. Srinivasan, "On graded electrode porosity as a design tool for improving the energy density of batteries," *Journal of The Electrochemical Society*, vol. 163, no. 3, A406–A416, 2016.

[33] M. Yao, K. Okuno, T. Iwaki, M. Kato, S. Tanase, K. Emura, and T. Sakai, "Lifepo 4-based electrode using micro-porous current collector for high power lithium ion battery," *Journal of Power Sources*, vol. 173, no. 1, pp. 545–549, 2007.

[34] M. Tian, W. Wang, Y. Liu, K. L. Jungjohann, C. T. Harris, Y.-C. Lee, and R. Yang, "A three-dimensional carbon nano-network for high performance lithium ion batteries," *Nano Energy*, vol. 11, pp. 500–509, 2015.

[35] Battery Univeristy, *Bu-106: Advantages of primary batteries*, Accessed: April 25, 2017. [Online]. Available: http://batteryuniversity.com/learn/article/primary_batteries.

[36] MEV Team, "A guide to understanding battery specifications," 2008.

[37] D. Deng, M. G. Kim, J. Y. Lee, and J. Cho, "Green energy storage materials: Nanostructured tio 2 and sn-based anodes for lithium-ion batteries," *Energy & Environmental Science*, vol. 2, no. 8, pp. 818–837, 2009.

[38] T. Huria, "Rechargeable lithium battery energy storage systems for vehicular applications," 2012.

[39] Battery Univeristy, *BU-205: Types of Lithium-ion*, Accessed: April 25, 2017. [Online]. Available: http://batteryuniversity.com/learn/article/types_of_lithium_ion.

[40] J. B. Goodenough and Y. Kim, "Challenges for rechargeable li batteries," *Chemistry of Materials*, vol. 22, no. 3, p. 587, 2010.

[41] R. Spotnitz, "Simulation of capacity fade in lithium-ion batteries," *Journal of Power Sources*, vol. 113, no. 1, pp. 72–80, 2003.

[42] *Capacity fade of a lithium-ion Battery*, Accessed: April 26, 2017. [Online]. Available: https://www.comsol.com/model/capacity-fade-of-a-lithium-ion-battery-12667.

[43] P. Arora, R. E. White, and M. Doyle, "Capacity fade mechanisms and side reactions in lithium-ion batteries," *Journal of the Electrochemical Society*, vol. 145, no. 10, pp. 3647–3667, 1998.

[44] J. H. Seo, J. Park, G. Plett, and A. M. Sastry, "Gas-evolution induced volume fraction changes and their effect on the performance degradation of li-ion batteries," *Electrochemical and Solid-State Letters*, vol. 13, no. 9, A135–A137, 2010.

[45] Y. Dai, L. Cai, and R. E. White, "Capacity fade model for spinel limn2o4 electrode," *Journal of The Electrochemical Society*, vol. 160, no. 1, A182–A190, 2013.

[46] Q. Sa and Y. Wang, "Ni foam as the current collector for high capacity c–si composite electrode," *Journal of Power Sources*, vol. 208, pp. 46–51, 2012.

[47] Z. Li, "Finite difference methods basics," *report, Center for Research in Scientific Computation & Department of Mathematics, North Carolina State University*, 2009.

[48] J. Newman and W. Tiedemann, "Porous-electrode theory with battery applications," *AIChE Journal*, vol. 21, no. 1, pp. 25–41, 1975.

[49] P Ramadass, B. Haran, R. White, and B. N. Popov, "Mathematical modeling of the capacity fade of li-ion cells," *Journal of Power Sources*, vol. 123, no. 2, pp. 230–240, 2003.

[50] R. Ghimire Prasad, "Improve the performance of a lithium ion battery by fabricating and using porous copper as a current collector," South Dakota State University, unpublished, 2017.

[51] Q. Zhang and R. E. White, "Comparison of approximate solution methods for the solid phase diffusion equation in a porous electrode model," *Journal of power sources*, vol. 165, no. 2, pp. 880–886, 2007.

[52] O. Barbarisi, F. Vasca, and L. Glielmo, "State of charge kalman filter estimator for automotive batteries," *Control Engineering Practice*, vol. 14, no. 3, pp. 267–275, 2006.

[53] J. Prins-Jansen, J. D. Fehribach, K. Hemmes, and J. De Wit, "A three-phase homogeneous model for porous electrodes in molten-carbonate fuel cells," *Journal of The Electrochemical Society*, vol. 143, no. 5, pp. 1617–1628, 1996.

[54] M. W. Verbrugge and B. J. Koch, "Electrochemical analysis of lithiated graphite anodes," *Journal of The Electrochemical Society*, vol. 150, no. 3, A374–A384, 2003.

[55] C. Speltino, D. Di Domenico, G. Fiengo, and A Stefanopoulou, "Comparison of reduced order lithium-ion battery models for control applications," in *Decision and Control, 2009 held jointly with the 2009 28th Chinese Control Conference. CDC/CCC 2009. Proceedings of the 48th IEEE Conference on*, IEEE, 2009, pp. 3276–3281.

[56] D. Di Domenico, G. Fiengo, and A. Stefanopoulou, "Lithium-ion battery state of charge estimation with a kalman filter based on a electrochemical model," in *Control Applications, 2008. CCA 2008. IEEE International Conference on*, IEEE, 2008, pp. 702–707.

[57] K. A. Smith, C. D. Rahn, and C.-Y. Wang, "Control oriented 1d electrochemical model of lithium ion battery," *Energy Conversion and management*, vol. 48, no. 9, pp. 2565–2578, 2007.

[58] D Domenico, A. Stefanopoulou, and G Di Fiengo, "Psm: Lithium-ion battery state of charge (soc) and critical surface charge (csc) estimation using an electrochemical model-driven extended kalman filter," *submitted to a special issue of ASME Journal of Dynamic Systems, Measurements and Control*, 2009.

[59] M. Rashid and A. Gupta, "Mathematical model for combined effect of sei formation and gas evolution in li-ion batteries," *ECS Electrochemistry Letters*, vol. 3, no. 10, A95–A98, 2014.

[60] X.-G. Yang, Y. Leng, G. Zhang, S. Ge, and C.-Y. Wang, "Modeling of lithium plating induced aging of lithium-ion batteries: Transition from linear to nonlinear aging," *Journal of Power Sources*, vol. 360, pp. 28–40, 2017.

[61] P. Verma, P. Maire, and P. Novák, "A review of the features and analyses of the solid electrolyte interphase in li-ion batteries," *Electrochimica Acta*, vol. 55, no. 22, pp. 6332–6341, 2010.

[62] S. J. An, J. Li, C. Daniel, D. Mohanty, S. Nagpure, and D. L. Wood, "The state of understanding of the lithium-ion-battery graphite solid electrolyte interphase (sei) and its relationship to formation cycling," *Carbon*, vol. 105, pp. 52–76, 2016.

[63] R. V. Bugga and M. C. Smart, "Lithium plating behavior in lithium-ion cells," *ECS Transactions*, vol. 25, no. 36, pp. 241–252, 2010.

[64] A. V. Randall, R. D. Perkins, X. Zhang, and G. L. Plett, "Controls oriented reduced order modeling of solid-electrolyte interphase layer growth," *Journal of Power Sources*, vol. 209, pp. 282–288, 2012.

[65] R. Fu, "Modeling, validation and analysis of degradation processes of lithium ion polymer batteries," PhD thesis, 2014.

[66] T. I. Evans, T. Nguyen, and R. E. White, "A mathematical model of a lithium/thionyl chloride primary cell," *Journal of the Electrochemical Society*, vol. 136, no. 2, pp. 328–339, 1989.

[67] A. Rabbani, S. Jamshidi, and S. Salehi, "An automated simple algorithm for realistic pore network extraction from micro-tomography images," *Journal of Petroleum Science and Engineering*, vol. 123, pp. 164–171, 2014.

[68] Wikipedia, *Watershed (image processing)*, Accessed: May 5, 2017. [Online]. Available: https://en.wikipedia.org/wiki/Watershed_(image_processing).

[69] L. JÄNTSCHI and S. D. BOLBOACA, "Distribution fitting 2. pearson-fisher, kolmogorov-smirnov, anderson-darling, wilks-shapiro, cramer-von-misses and jarque-bera statistics," *Bulletin of University of Agricultural Sciences and Veterinary Medicine Cluj-Napoca. Horticulture*, vol. 66, no. 2, pp. 691–697, 2010.

[70] T. Ashwin, A. McGordon, and P. A. Jennings, "A mass transfer based variable porosity model with particle radius change for a lithium-ion battery," *Electrochimica Acta*, vol. 232, pp. 203–214, 2017.

[71] T.-J. Kuo, K.-Y. Lee, C.-K. Huang, J.-H. Chen, W.-L. Chiu, C.-F. Huang, and S.-D. Wu, "State of charge modeling of lithium-ion batteries using dual exponential functions," *Journal of Power Sources*, vol. 315, pp. 331–338, 2016.

[72] P Ramadass, B. Haran, R. White, and B. N. Popov, "Capacity fade of sony 18650 cells cycled at elevated temperatures: Part i. cycling performance," *Journal of power sources*, vol. 112, no. 2, pp. 606–613, 2002.

[73] C. Wang and V. Srinivasan, "Computational battery dynamics (cbd)—electrochemical/thermal coupled modeling and multi-scale modeling," *Journal of power sources*, vol. 110, no. 2, pp. 364–376, 2002.

[74] A. Smith, J. C. Burns, X. Zhao, D. Xiong, and J. Dahn, "A high precision coulometry study of the sei growth in li/graphite cells," *Journal of The Electrochemical Society*, vol. 158, no. 5, A447–A452, 2011.

[75] G. E. Blomgren, "Electrolytes for advanced batteries," *Journal of Power Sources*, vol. 81, pp. 112–118, 1999.

[76] T. Yoshida, M. Takahashi, S. Morikawa, C. Ihara, H. Katsukawa, T. Shiratsuchi, and J.-i. Yamaki, "Degradation mechanism and life prediction of lithium-ion batteries," *Journal of The Electrochemical Society*, vol. 153, no. 3, A576–A582, 2006.

[77] *State of Health (SOH) Determination*, Accessed: April 30, 2017. [Online]. Available: http://www.mpoweruk.com/soh.htm.

[78] X. Han, M. Ouyang, L. Lu, and J. Li, "Cycle life of commercial lithium-ion batteries with lithium titanium oxide anodes in electric vehicles," *Energies*, vol. 7, no. 8, pp. 4895–4909, 2014.

[79] M. Yao, K. Okuno, T. Iwaki, T. Awazu, and T. Sakai, "Long cycle-life lifepo 4/cu-sn lithium ion battery using foam-type three-dimensional current collector," *Journal of Power Sources*, vol. 195, no. 7, pp. 2077–2081, 2010.

[80] P. W. Northrop, V. Ramadesigan, S. De, and V. R. Subramanian, "Coordinate transformation, orthogonal collocation, model reformulation and simulation of electrochemical-thermal behavior of lithium-ion battery stacks," *Journal of The Electrochemical Society*, vol. 158, no. 12, A1461–A1477, 2011.

[81] T.-S. Dao, C. P. Vyasarayani, and J. McPhee, "Simplification and order reduction of lithium-ion battery model based on porous-electrode theory," *Journal of Power Sources*, vol. 198, pp. 329–337, 2012.

[82] T. Ashwin, Y. M. Chung, and J. Wang, "Capacity fade modelling of lithium-ion battery under cyclic loading conditions," *Journal of Power Sources*, vol. 328, pp. 586–598, 2016.